

Cooperative RIS and STAR-RIS Assisted mMIMO Communication: Analysis and Optimization

Anastasios Papazafeiropoulos , Senior Member, IEEE, Ahmet M. Elbir , Senior Member, IEEE, Pandelis Kourtessis , Ioannis Krikidis , Fellow, IEEE, and Symeon Chatzinotas , Fellow, IEEE

Abstract—Reconfigurable intelligent surface (RIS) has emerged as a cost-effective and promising solution to extend the wireless signal coverage and improve the performance via passive signal reflection. Different from existing works which do not account for the cooperation between RISs or do not provide full space coverage, we propose the marriage of cooperative double-RIS with simultaneously transmitting and reflecting RIS (STAR-RIS) technologies denoted as RIS/STAR-RIS under correlated Rayleigh fading conditions to assist the communication in a massive multiple-input multiple-output (mMIMO) setup. The proposed architecture is superior since it enjoys the benefits of the individual designs. We introduce a channel estimation approach of the cascaded channels with reduced overhead. Also, we obtain the deterministic equivalent (DE) of the downlink achievable sum spectral efficiency (SE) in closed form based on large-scale statistics. Notably, relied on statistical channel state information (CSI), we optimise both surfaces by means of the projected gradient ascent method (PGAM), and obtain the gradients in closed form. The proposed optimization achieves to maximise the sum SE of such a complex system, and has low complexity and low overhead since it can be performed at every several coherence intervals. Numerical results show the benefit of the proposed architecture and verify the analytical framework. In particular, we show that the RIS/STAR-RIS architecture outperforms the conventional double-RIS or its single-RIS counterparts.

Manuscript received 21 January 2023; revised 10 March 2023; accepted 30 March 2023. Date of publication 5 April 2023; date of current version 19 September 2023. The work of Anastasios Papazafeiropoulos was supported by the University of Hertfordshire's 5-year Vice Chancellor's Research Fellowship. The work of Symeon Chatzinotas was supported by the National Research Fund, Luxembourg through the Project RISOTTI. This work was supported in part by the European Regional Development Fund and the Republic of Cyprus through the Research and Innovation Foundation through the Project INFRASTRUCTURES/1216/0017 (IRIDA), and in part by the European Research Council (ERC) through the European Union's Horizon 2020 Research and Innovation Programme under Grant 819819. The review of this article was coordinated by Dr. H. Zhang. (Corresponding author: Anastasios Papazafeiropoulos.)

Anastasios Papazafeiropoulos is with the Communications and Intelligent Systems Research Group, University of Hertfordshire, AL10 9AB Hatfield, U.K., and also with the SnT at the University of Luxembourg, 1855 Esch-sur-Alzette, Luxembourg (e-mail: tapapazaf@gmail.com).

Ahmet M. Elbir is with the Interdisciplinary Centre for Security, Reliability, and Trust (SnT), University of Luxembourg, 1855 Esch-sur-Alzette, Luxembourg, and also with Duzce University, 81620 Duzce, Turkey (e-mail: ahmetmelbir@gmail.com).

Pandelis Kourtessis is with the Communications and Intelligent Systems Research Group, University of Hertfordshire, AL10 9AB Hatfield, U.K. (e-mail: p.kourtessis@herts.ac.uk).

Ioannis Krikidis is with the IRIDA Research Centre for Communication Technologies, Department of Electrical and Computer Engineering, University of Cyprus, 1678 Nicosia, Cyprus (e-mail: krikidis.ioannis@ucy.ac.cy).

Symeon Chatzinotas is with the SnT, University of Luxembourg, 1855 Esch-sur-Alzette, Luxembourg (e-mail: schatzin@ieee.org).

Digital Object Identifier 10.1109/TVT.2023.3264724

Index Terms—Double-RIS, simultaneously transmitting and reflecting RIS, correlated Rayleigh fading, spectral efficiency, 6G networks.

I. INTRODUCTION

BASED on the recent advancements in metasurfaces, reconfigurable intelligent surface (RIS) has emerged as a promising technology to actualise a smart and reconfigurable radio environment through passive beamforming (PB) [1], [2]. RIS consists of a large number of nearly passive elements, each of which can be independently adjusted to modify in real time the amplitude/phase shift of the impinging signal [3]. The intelligent adjustment of its elements, enables RIS to proactively configure the wireless propagation channel towards better signal transmission instead of adapting to the channel by standard transceiver techniques. Among its benefits, we meet its low hardware cost as well as its lightweight and conformal geometry that can promote a large-scale and flexible deployment of RIS [1], [2].

These attractive characteristics of RIS have attracted the interest from both academia and industry in studying the performance under various wireless system setups such as massive multiple-input-multiple-output (mMIMO) communication [4], [5], orthogonal frequency division multiplexing (OFDM) [6], [7], relaying communication [8], [9], non-orthogonal multiple access (NOMA) [10], double/multi-RIS network [11], [12], [13], [14], [15], [16], [17], [18]. In particular, the double-RIS implementation is an interesting research direction providing enhanced coverage and better performance due to the multiplied beamforming gain [11]. However, most existing works on RIS have focused on setups with one or more independently distributed RISs that serve user equipments (UEs) by simple reflection only without considering the cooperation among multiple RISs. In the case of double-RIS, the PB over multiple RISs should be designed cooperatively, which means exploitation of the multiplied beamforming gain while avoiding the undesired interference to improve the system performance [11], [12]. In [11], it was shown that a PB gain of order $\mathcal{O}(N^4)$ can be obtained, where N is the total number of elements of the two cooperative RISs. This result outperforms the conventional single-RIS with a PB gain of order $\mathcal{O}(N^2)$ [3]. Notably, the implementation of two cooperative RISs induces additional path loss, which can be compensated by a sufficiently large number of N . Although [19] presented this promising result, it relied on an ideal line-of-sight (LoS) inter-RIS channel and a simplified

system with a single antenna base station (BS), a single UE, and no single-reflection links. In [11], the problem of addressing a general setup with arbitrary channels and with multiple BS antennas/UEs was considered but does not provide full-space coverage.

In parallel, most existing RIS research contributions assume that RISs can only reflect impinging waves which henceforth will be referred to as conventional single RISs. This design assumes that both the transmitter and the receiver are located on the same side of the surface, which results in half-space coverage and restricts the flexibility of the RIS technology since UEs may be located on both sides of the surface. To cover this gap, a new concept referred to as simultaneously transmitting and reflecting RIS (STAR-RIS) was presented in [20], [21], [22], [23], [24], [25]. The works [26], [27] are among the first, where the feasibility of STAR-RIS was experimentally verified. According to STAR-RIS, the incident signal on a STAR-RIS element is divided into parts that correspond to the reflected and transmitted signals. In the former case, the signal is reflected to the same space as the impinging signal, while, in the latter case, the signal is transmitted to the opposite space. This is achieved by the manipulation of magnetic and electric currents of the surface elements that enable the reconfiguration of the transmitted and reflected signals through generally independent coefficients denoted as transmission and reflective coefficients [20], [21]. Despite its advantages, the literature concerning the integration of STAR-RIS into wireless communication systems is still limited [20], [21], [22], [23], [24], [25]. For example, in [21], practical operation protocols for STAR-RIS have been proposed, and the joint transmission and reflection beamforming design for unicast and multicast communication has been investigated. Also, in [22], the impact of correlated Rayleigh fading was studied in STAR-RIS-assisted full duplex systems. Note that intelligent omni-surface (IOS), proposed in [28], is a similar idea to STAR-RIS, but the phase shifts for transmission and reflection are identical.

Contributions: The main contribution of this paper are summarised as follows:

- Motivated by the above observations, we propose a double-RIS architecture, where the first and second surfaces consist of a conventional RIS and a STAR-RIS based on the energy splitting (ES) protocol, respectively. Contrary to [11], the marriage of the double-RIS with the STAR-RIS combines their advantages. The double-RIS design aims mainly to extend the coverage, and the STAR-RIS aims to provide 360° coverage near the receiver side, while increasing the sum-rate. Specifically, two distributed surfaces are deployed near the mMIMO BS and the group of nearby UEs to enhance communication. UEs can be located on both sides of the second surface (STAR-RIS). Note that we account for both single and double links as well as correlated Rayleigh fading.
- The introduction of the STAR-RIS in the double-RIS architecture emerges certain difficulties in the statistical analysis, channel estimation, and PB optimization. In particular, contrary to other works on STAR-RIS, we have achieved a unified analysis regarding the channel estimation and

data transmission phase that applies to a UE found in any of the t or r regions. Specifically, we consider an uplink training phase to obtain the imperfect CSI in closed-form for all links. Based on the deterministic equivalent (DE) analysis, which is often used in mMIMO systems, we derive in closed-form the downlink achievable signal-to-interference-plus-noise ratio (SINR) and the sum spectral efficiency (SE) being dependent on large-scale statistics. Also, contrary to many works that have relied on independent fading such as [3], [29], we have assumed correlated fading, which is unavoidable in practice and affects the performance [30].

- Given this system and based on statistical CSI, we optimize the PBs at the two surfaces to maximise the same rate. To the best of our knowledge, we are the first to optimize simultaneously the amplitudes and the phase shifts of the PB in a STAR-RIS system. This is a significant contribution since other works optimize only the phase shifts or optimize both the amplitudes and the phase shifts in an alternating optimization manner. Notably, this property is important for STAR-RIS applications, which have twice the number of optimization variables compared to reflecting-only RIS. In particular, since we can derive the gradients in closed form simple expressions, we apply the projected gradient ascent method (PGAM) alternatively for each surface, and obtain the corresponding optimal PB in closed form while achieving low complexity and low overhead. The main reason is that the optimization can take place at every several coherence intervals when the statistical CSI changes.
- We provide Monte-Carlo (MC) simulations to corroborate the theoretical results on the RIS/STAR-RIS performance and investigate the effectiveness of the proposed optimization of PB. It is shown that the RIS/STAR-RIS can achieve significant performance gains over the conventional double-RIS and single-RIS or STAR-RIS architectures.

Paper Outline: The rest of this paper is organised as follows. Section II presents the system model of the proposed RIS/STAR-RIS architecture. In Section III, we provide the channel estimation approach. In Section IV, we derive the DE of the downlink sum SE. In Section V, we design the RIS PB for each surface and study its performance. Simulations results are presented in Section VI to assess the performance of the proposed design and validate the analytical. Finally, Section VII concludes the paper.

Notation: Vectors and matrices are denoted by boldface lower and upper case symbols, respectively. The notations $(\cdot)^T$, $(\cdot)^H$, and $\text{tr}(\cdot)$ describe the transpose, Hermitian transpose, and trace operators, respectively. Moreover, the notations $\mathbb{E}[\cdot]$ and $\text{Var}(\cdot)$ express the expectation and variance operators, respectively. The notation $\text{diag}(\mathbf{A})$ describes a vector with elements equal to the diagonal elements of \mathbf{A} , the notation $\text{diag}(\mathbf{x})$ describes a diagonal matrix whose elements are \mathbf{x} , while $\mathbf{b} \sim \mathcal{CN}(\mathbf{0}, \mathbf{\Sigma})$ describes a circularly symmetric complex Gaussian vector with zero mean and a covariance matrix $\mathbf{\Sigma}$. Also, the notation $a_n \asymp b_n$ with a_n and b_n being two infinite sequences denotes almost sure

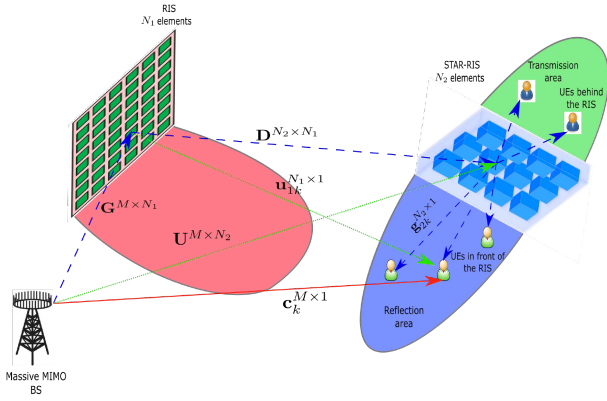


Fig. 1. mMIMO RIS/STAR-RIS assisted system with multiple UEs at transmission and reflection regions.

convergence as $M \rightarrow \infty$, and the notation $\frac{\partial f(x)}{\partial x}$ denotes the partial derivative of f with respect to x .

II. SYSTEM MODEL

We consider a mixed double-RIS cooperatively assisted multi-user MIMO communication system, where two distributed RISs assist the communication from an M -antenna mMIMO BS to K single-antenna UEs, as shown in Fig. 1. The surface, positioned near the BS is denoted as RIS 1, and plays the role of an extender. The second surface, being a STAR-RIS (denoted as RIS 2), can be located close to the UEs, which can be distributed on both sides of the surface such as indoor and outdoor UEs by providing 360° coverage.¹ In particular, $\mathcal{K}_r \in \{1, \dots, K_r\}$ UEs are located in the reflection region (r) and $\mathcal{K}_t \in \{1, \dots, K_t\}$ UEs are located in the transmission region (t) of the STAR-RIS, where $K_t + K_r = K$. Moreover, we denote by $\mathcal{W}_k = \{w_1, w_2, \dots, w_K\}$ the operation mode for the STAR-RIS for each of the K UEs. Specifically, if the k th UE is in the reflection region, i.e., $k \in \mathcal{K}_r$ then $w_k = r$, otherwise, it will be $w_k = t$. We assume that surfaces 1 and 2 consist of uniform planar arrays (UPAs) of N_1 and N_2 passive elements, respectively, which means $N_1 + N_2 = N$. The corresponding sets are denoted as \mathcal{N}_1 and \mathcal{N}_2 . Also, each distributed RIS is connected to a smart controller that adjusts its amplitudes/phase shifts and exchanges information with the BS via a separate reliable wireless link. The RIS elements of both surfaces can be perfectly controlled. Despite the presence of blockages, we assume the general scenario, where direct links exist.

We assume that the STAR-RIS can configure the transmitted (t) and reflected (r) signals by two independent coefficients. Specifically, let $t_n = (\beta_n^t e^{j\phi_n^t})s_n$ and $r_n = (\beta_n^r e^{j\phi_n^r})s_n$ denote the transmitted and reflected signal by the n th element of the STAR-RIS, respectively. Regarding the amplitude and phase parameters, we have $\beta_n^{w_k} \in [0, 1]$ and $\phi_n^{w_k} \in [0, 2\pi)$. According to this model ϕ_n^t and ϕ_n^r can be chosen independently. However,

¹If the first reflection-only RIS is substituted by a STAR-RIS, the second STAR-RIS could be placed at the reflection or the transmission region, which leads to differences between these two scenarios. This research direction will be the topic of future research.

the choice of amplitudes is based on the relationship provided by the law of energy conservation as

$$(\beta_n^t)^2 + (\beta_n^r)^2 = 1, \forall n = 1, \dots, N_2. \quad (1)$$

Furthermore, in the case of the conventional RIS, i.e., RIS 1, $\Phi_1 = \text{diag}(\alpha_1 e^{j\varphi_1}, \dots, \alpha_N e^{j\varphi_N}) \in \mathbb{C}^{N_1 \times N_1}$ is the diagonal PB that expresses the response of N_1 elements with $\varphi_n \in [0, 2\pi]$ and $\alpha_n \in [0, 1]$ describing the phase and amplitude coefficient for element $n = 0, \dots, N_1$, respectively. Without loss of generality, we make the common assumption of maximum reflection ($\alpha_n = 1 \forall n$) based on recent advances in lossless metasurfaces [31], because we want to focus on the operation and novel optimization of the STAR-RIS. The generalization to not optimal reflection for RIS 1 is straightforward and can follow similar lines to the STAR-RIS optimization.

A. Operation for STAR-RIS

Our study concerns the ES protocol [21], which is summarized below. The study of the mode switching (MS) protocol is left for future work.

ES protocol: All elements of STAR-RIS serve simultaneously K UEs. Especially, the PB is expressed as $\Phi_{2,w_k}^{\text{ES}} = \text{diag}(\beta_1^{w_k} e^{j\phi_1^{w_k}}, \dots, \beta_{N_2}^{w_k} e^{j\phi_{N_2}^{w_k}}) \in \mathbb{C}^{N_2 \times N_2}$, where $\beta_n^{w_k} \geq 0$, $(\beta_n^t)^2 + (\beta_n^r)^2 = 1$, and $|e^{j\phi_n^{w_k}}| = 1, \forall n = 1, \dots, N_2$.

Henceforth, for the sake of exposition, we set $\bar{\theta}_n = e^{j\varphi_n}, n \in \mathcal{N}_1$ and $\theta_n^{w_k} = e^{j\phi_n^{w_k}}, n \in \mathcal{N}_2$. Also, we denote $\bar{\theta} = \text{diag}(\Phi_1) = [\bar{\theta}_1, \dots, \bar{\theta}_{N_1}]^T \in \mathbb{C}^{N_1 \times 1}$, $\theta^u = [\theta_1^u, \dots, \theta_{N_2}^u]^T \in \mathbb{C}^{N_2 \times 1}$, and $\beta^u = [\beta_1^u, \dots, \beta_{N_2}^u]^T \in \mathbb{C}^{N_2 \times 1}$, where $u = \{t, r\}$.

B. Channel Model

Based on a narrowband quasi-static block-fading model with independent channel realizations across different coherence blocks, we denote $\mathbf{G}_1 = [\mathbf{g}_{11} \dots, \mathbf{g}_{1N_1}] \in \mathbb{C}^{M \times N_1}$, $\mathbf{D} \in \mathbb{C}^{N_2 \times N_1}$, $\mathbf{g}_{2k} \in \mathbb{C}^{N_2 \times 1}$, $\mathbf{u}_{1k} \in \mathbb{C}^{N_1 \times 1}$, $\mathbf{U}_2 = [\mathbf{u}_{21} \dots, \mathbf{u}_{2N_2}] \in \mathbb{C}^{M \times N_2}$, and $\mathbf{c}_k \in \mathbb{C}^{M \times 1}$ as the channels from the BS to RIS, from RIS to STAR-RIS, from RIS to UE k , from the BS to the STAR-RIS, and the direct link between the BS and UE k , respectively. By taking into account correlated Rayleigh fading and path-loss,² we have

$$\text{vec}(\mathbf{G}_1) \sim \mathcal{CN}(\mathbf{0}, \mathbf{R}_{t1}), \quad (2)$$

$$\text{vec}(\mathbf{D}) \sim \mathcal{CN}(\mathbf{0}, \mathbf{R}_{12}), \quad (3)$$

$$\mathbf{g}_{2k} \sim \mathcal{CN}(\mathbf{0}, \mathbf{R}_{2k}), \quad (4)$$

$$\mathbf{u}_{1k} \sim \mathcal{CN}(\mathbf{0}, \mathbf{R}_{1k}), \quad (5)$$

$$\text{vec}(\mathbf{U}_2) \sim \mathcal{CN}(\mathbf{0}, \mathbf{R}_{t2}), \quad (6)$$

$$\mathbf{c}_k \sim \mathcal{CN}(\mathbf{0}, \bar{\beta}_k \mathbf{R}_t), \quad (7)$$

where $\mathbf{R}_{t1} = \beta_{t1} \mathbf{R}_t \otimes \mathbf{R}_1 \in \mathbb{C}^{MN_1 \times MN_1}$, $\mathbf{R}_{12} = \beta_{12} \mathbf{R}_1 \otimes \mathbf{R}_2 \in \mathbb{C}^{N_1 N_2 \times N_1 N_2}$, $\mathbf{R}_{2k} = \beta_{2k} \mathbf{R}_2 \in \mathbb{C}^{N_2 \times N_2}$, $\mathbf{R}_{1k} = \beta_{1k} \mathbf{R}_1 \in \mathbb{C}^{N_1 \times N_1}$, and $\mathbf{R}_{t2} = \beta_{t2} \mathbf{R}_t \otimes \mathbf{R}_2 \in \mathbb{C}^{MN_2 \times MN_2}$ are the spatial covariance matrices of the respective links with β_{t1} , β_{12} ,

²The analysis, corresponding to correlated Rician fading, where an LoS component exists additionally to a multipath part, is the topic of future work.

β_{2k} , β_{1k} , β_{t2} , and $\bar{\beta}_k$ being the corresponding path-losses. Also, $\mathbf{R}_t \in \mathbb{C}^{M \times M}$ is the correlation matrix at the BS, while $\mathbf{R}_1 \in \mathbb{C}^{N_1 \times N_1}$ and $\mathbf{R}_2 \in \mathbb{C}^{N_2 \times N_2}$ are the correlation matrices of RIS and STAR-RIS, respectively. Regarding \mathbf{R}_t , it can be modeled e.g., as in [32], and \mathbf{R}_1 , \mathbf{R}_2 are modeled as in [30], which describes isotropic Rayleigh fading. Specifically, let $d_{q,V}$ and $d_{q,H}$ denote the vertical height and horizontal width of each element of RIS $q = 1, 2$, where RIS 1 and RIS 2 correspond to the conventional RIS and STAR-RIS, respectively. Then, the (i, j) th element of the representative correlation matrix $\mathbf{R}_q \in \mathbb{C}^{N_q \times N_q}$ in (2)–(7) in the case of a RIS with $N_q = N_{q,H}N_{q,V}$ elements is given by

$$r_{q,ij} = d_{q,H}d_{q,V} \text{sinc}(2\|\mathbf{u}_i - \mathbf{u}_j\|/\lambda), \quad (8)$$

where $\mathbf{u}_\epsilon = [0, \text{mod}(\epsilon - 1, N_{q,H})d_{q,H}, [(\epsilon - 1)/N_{q,V}]d_{q,V}]^T$, $\epsilon \in \{i, j\}$, and λ is the wavelength of the plane wave, while $N_{q,H}$ and $N_{q,V}$ denote the horizontally and vertically passive elements of RIS q , i.e., $N_q = N_{q,H} \times N_{q,V}$. Note that the path-losses and the covariance matrices are assumed known since they can be obtained with practical methods, e.g., see [33].

With fixed PBs, the aggregated channel vector for UE k via both RISs is

$$\mathbf{h}_k = \mathbf{d}_k + \mathbf{G}_1 \Phi_1 \mathbf{D} \Phi_{2,w_k} \mathbf{g}_{2k}, \quad (9)$$

and has a variance $\mathbf{R}_{0k} = \mathbb{E}\{\mathbf{h}_k \mathbf{h}_k^H\}$. We have

$$\begin{aligned} \mathbf{R}_{0k} &= \bar{\beta}_k \mathbf{R}_t + \beta_{2k} \mathbb{E}\{\mathbf{G}_1 \Phi_1 \mathbf{D} \Phi_{2,w_k} \mathbf{R}_{2k} \Phi_{2,w_k}^H \mathbf{D}^H \Phi_1^H \mathbf{G}_1^H\} \\ &= \bar{\beta}_k \mathbf{R}_t + \beta_{2k} \beta_{12} \text{tr}(\mathbf{R}_1 \Phi_{2,w_k} \mathbf{R}_2 \Phi_{2,w_k}^H) \mathbb{E}\{\mathbf{G}_1 \Phi_1 \mathbf{R}_2 \Phi_1^H \mathbf{G}_1^H\} \\ &= \bar{\beta}_k \mathbf{R}_t + \hat{\beta}_k \text{tr}(\mathbf{R}_1 \Phi_{2,w_k} \mathbf{R}_2 \Phi_{2,w_k}^H) \text{tr}(\mathbf{R}_1 \Phi_1 \mathbf{R}_2 \Phi_1^H) \mathbf{R}_t, \end{aligned} \quad (12)$$

where, in (10) we have relied on the independence between \mathbf{c}_k , \mathbf{G}_1 , \mathbf{D} , and \mathbf{g}_{2k} , and have applied $\mathbb{E}\{\mathbf{g}_{2k} \mathbf{g}_{2k}^H\} = \beta_{2k} \mathbf{R}_{\text{RIS}}$. In (11), we have expressed \mathbf{D} in terms of its equivalent notation $\mathbf{D} = \sqrt{\beta_{12}} \mathbf{R}_2^{1/2} \tilde{\mathbf{D}} \mathbf{R}_1^{1/2}$ with $\text{vec}(\tilde{\mathbf{D}}) \sim \mathcal{CN}(\mathbf{0}, \mathbf{I}_{N_1 N_2})$, and we have applied the property $\mathbb{E}\{\mathbf{V} \mathbf{U} \mathbf{V}^H\} = \text{tr}(\mathbf{U}) \mathbf{I}_M$ with \mathbf{U} being a deterministic square matrix, and \mathbf{V} being any matrix with independent and identically distributed (i.i.d.) entries of zero mean and unit variance. In (12), we have set $\hat{\beta}_k = \beta_{t1} \beta_{2k} \beta_{12}$, we have expressed \mathbf{G}_1 in terms of its equivalent notation $\mathbf{G}_1 = \sqrt{\beta_{t1}} \mathbf{R}_1^{1/2} \tilde{\mathbf{G}} \mathbf{R}_t^{1/2}$ with $\text{vec}(\tilde{\mathbf{G}}) \sim \mathcal{CN}(\mathbf{0}, \mathbf{I}_{M N_1})$, and we have applied again the previous property. It is worthwhile to mention that, when $\mathbf{R}_1 = \mathbf{I}_{N_1}$, and $\mathbf{R}_2 = \mathbf{I}_{N_2}$, \mathbf{R}_{0k} does not depend on the phase shifts but only on the amplitudes, as also observed in [34]. In other words, \mathbf{R}_{0k} can be optimized only with respect to the amplitudes.

Given a fixed PB each time for the single links BS-STAR-RIS-UE k and BS-RIS-UE k , the cascaded channels are $\mathbf{h}_{2k} = \mathbf{U}_2 \Phi_{2,w_k} \mathbf{g}_{2k}$ and $\mathbf{h}_{1k} = \mathbf{G}_1 \Phi_1 \mathbf{u}_{1k}$ with variances $\mathbf{R}_{2k} = \mathbb{E}\{\mathbf{h}_{2k} \mathbf{h}_{2k}^H\}$ and $\mathbf{R}_{1k} = \mathbb{E}\{\mathbf{h}_{1k} \mathbf{h}_{1k}^H\}$, respectively. In particular, these can be written as

$$\mathbf{R}_{2k} = \hat{\beta}_{2k} \text{tr}(\mathbf{R}_t \Phi_{2,w_k} \mathbf{R}_2 \Phi_{2,w_k}^H) \mathbf{R}_2, \quad (13)$$

$$\mathbf{R}_{1k} = \hat{\beta}_{1k} \text{tr}(\mathbf{R}_t \Phi_1 \mathbf{R}_1 \Phi_1^H) \mathbf{R}_1, \quad (14)$$

where $\hat{\beta}_{2k} = \beta_{2k} \beta_{t2}$ and $\hat{\beta}_{1k} = \beta_{1k} \beta_{t1}$. Note that we have used similar steps to (12) to obtain (13) and (14), and have considered \mathbf{U}_2 in terms of its equivalent notation $\mathbf{U}_2 = \sqrt{\beta_{t2}} \mathbf{R}_2^{1/2} \tilde{\mathbf{U}} \mathbf{R}_t^{1/2}$ with $\text{vec}(\tilde{\mathbf{U}}) \sim \mathcal{CN}(\mathbf{0}, \mathbf{I}_{M N_2})$.

Remark 1: Under independent Rayleigh fading conditions, i.e., $\mathbf{R}_1 = \mathbf{I}_{N_1}$, $\mathbf{R}_2 = \mathbf{I}_{N_2}$, and $\mathbf{R}_t = \mathbf{I}_M$, the variances of cascaded channels become $\mathbf{R}_{0k} = \hat{\beta}_k N_1 \sum_{i=1}^{N_2} (\beta_i^{w_k})^2 \mathbf{I}_M$, $\mathbf{R}_{1k} = \hat{\beta}_{2k} \sum_{i=1}^{N_2} (\beta_i^{w_k})^2 \mathbf{I}_{N_2}$, and $\mathbf{R}_{2k} = \hat{\beta}_{2k} N_1 \mathbf{I}_{N_1}$, which are independent of the phase shifts. Hence, the correlation matrices appear dependence only on the amplitudes of the STAR-RIS. In this case, the optimization provided below, which is based on statistical CSI, takes place only with respect to the amplitudes of the second surface, while no phase shifts optimization can be performed. However, given that correlated fading is unavoidable in practice, the optimization of the surfaces depends on the phase shifts in real-world scenarios.

III. CHANNEL ESTIMATION

In practice, CSI is imperfect. Herein, we rely on the time division duplex (TDD) protocol to estimate the channels by an uplink training phase with pilot symbols [35]. However, both RISs, consisting of nearly passive elements without any RF chains, cannot obtain the received pilots by UEs and process the estimated channels. Generally, there are two approaches for channel estimation that correspond to the estimation of the individual channels [3], [6], [11], and to the estimation of the aggregated channels by using long-term performance metrics [4], [5], [36]. The advantages of the latter approach are the implementation without any extra hardware and with low power cost. Hence, we follow the standard approach in mMIMO systems to estimate the cascaded channels, which requires less hardware and lower complexity compared to estimating the individual channels. Actually, one of the advantages of this work is to make the expression for the channel estimation “looking” identical for both types of users belonging to different areas of the second RIS but note that at the end it is different since \mathbf{R}_k including the expressions corresponding to the phases shifts is different, for users in t and r regions. In other words, we have achieved to introduce the standard channel estimation for multiple-user SIMO to STAR-RIS, which has not taken place before. However, there is a cost compared to the instantaneous performance. If we focused on short-term metrics such as instantaneous SE, then the effective cascaded channels should be estimated by tuning the RIS passive beamforming (rather than fixed).³

Although the transmitted signal from UE k can propagate along both channels simultaneously, the double-RIS channel and single-RIS channel can be estimated separately. Specifically, first, the single-RIS channels are estimated by switching off the other RIS. Next, we can remove the single-RIS links by carefully selecting the pilots, as was performed in [36, Eq. 8]. Note that by picking good pilots, we can also remove the double-RIS-aided link from the total channel without turning off the individual RIS as well.

³In the case we would like to acquire the individual channels, we could assume receive RF chains integrated into the RISs similar to [8], [12].

The following analysis achieves to obtain the estimated channels for fixed PBs in closed-forms in terms of large-scale statistics, and thus, channel estimation can be performed at every several coherence intervals. Other methods such as [37] do not provide analytical expressions while not capturing the correlation effect since they obtain the estimated channel per RIS element [38].

In this direction, we assume that each block has a duration of τ_c channel uses, where τ channel uses are allocated for the uplink training phase and $\tau_c - \tau$ channel uses are allocated for the downlink data transmission phase.

For the double-RIS-assisted channels, we assume that all UEs either in t or r region of the STAR-RIS send orthogonal pilot sequences. Given that the duration of the uplink training phase is τ channel uses, we denote by $\mathbf{x}_k = [x_{k,1}, \dots, x_{k,\tau}]^T \in \mathbb{C}^{\tau \times 1}$ the pilot sequence of UE k that can be located in any of the two regions. Thus, we assume that all UEs from both regions send pilots to the BS, which receives

$$\mathbf{Y}^{\text{tr}} = \sum_{i=1}^K \mathbf{h}_i \mathbf{x}_i^H + \mathbf{Z}^{\text{tr}}, \quad (15)$$

where $\mathbf{Z}^{\text{tr}} \in \mathbb{C}^{M \times \tau}$ is the received AWGN matrix having independent columns with each one distributed as $\mathcal{CN}(\mathbf{0}, \sigma^2 \mathbf{I}_M)$. Next, we multiply (15) with the transmit training sequence from UE k to remove the interference from other UEs, which can be located in the same or the opposite region, and we obtain

$$\mathbf{r}_k = \mathbf{h}_k + \frac{\mathbf{z}_k}{\tau P}, \quad (16)$$

where $\mathbf{z}_k = \mathbf{Z}^{\text{tr}} \mathbf{x}_k$.

Lemma 1: The linear minimum mean square error (LMMSE) estimate of the double-RIS-assisted channel \mathbf{h}_k between UE k and the BS is written as

$$\hat{\mathbf{h}}_k = \mathbf{R}_{0k} \mathbf{Q}_{0k} \mathbf{r}_k, \quad (17)$$

where $\mathbf{Q}_{0k} = (\mathbf{R}_{0k} + \frac{\sigma^2}{\tau P} \mathbf{I}_M)^{-1}$, and \mathbf{r}_k is the noisy channel given by (16).

Proof: Please see Appendix A. ■

According to the property of the orthogonality of LMMSE estimation, the overall perfect channel can be written in terms of the estimated channel $\hat{\mathbf{h}}_k$ and estimation channel error vectors $\tilde{\mathbf{h}}_k$ as

$$\mathbf{h}_k = \hat{\mathbf{h}}_k + \tilde{\mathbf{h}}_k, \quad (18)$$

where $\hat{\mathbf{h}}_k$ and $\tilde{\mathbf{h}}_k$ are uncorrelated, have zero mean, and variances (cf. (52)) $\Psi_k = \mathbf{R}_{0k} \mathbf{Q}_{0k} \mathbf{R}_{0k}$ and $\mathbf{E}_k = \mathbf{R}_{0k} - \Psi_k$, respectively.

Regarding the estimation of the single-RIS-assisted channels, we provide the following lemma.

Lemma 2: The LMMSE estimate of the single-RIS-assisted channels \mathbf{h}_{ik} for $i = 1, 2$ between UE k obeys to

$$\mathbf{h}_{ik} = \hat{\mathbf{h}}_{ik} + \tilde{\mathbf{h}}_{ik}, \quad i = 1, 2 \quad (19)$$

where $\hat{\mathbf{h}}_{ik}$ and $\tilde{\mathbf{h}}_{ik}$ are uncorrelated, have zero mean, and variances $\Psi_{ik} = \mathbf{R}_{ik} \mathbf{Q}_{ik} \mathbf{R}_{ik}$ and $\mathbf{E}_{ik} = \mathbf{R}_{ik} - \Psi_{ik}$, respectively.

Proof: The proof follows similar lines with the proof of Lemma 1. ■

Remark 2: We have followed a typical approach for channel estimation because it presents several advantages: i) This method provides the estimated cascaded channel vectors in closed-forms, while other methods such as [37] do not result in closed-form expressions; ii) Channel estimation can be performed at every several coherence intervals since the estimated channels depend on large-scale statistics.

With the above setup, the superimposed channel from the BS to UE k , which includes the double-reflection link (BS \rightarrow RIS \rightarrow STAR-RIS \rightarrow UE k) and the two single-reflection links (BS \rightarrow RIS \rightarrow UE k) and (BS \rightarrow STAR-RIS \rightarrow UE k) is written as

$$\begin{aligned} \bar{\mathbf{h}}_k &= \mathbf{h}_k + \mathbf{h}_{1k} + \mathbf{h}_{2k} \\ &= \mathbf{c}_k + \mathbf{G}_1 \Phi_1 \mathbf{D} \Phi_2 \mathbf{g}_{2k} + \mathbf{G}_1 \Phi_1 \mathbf{u}_{1k} + \mathbf{U}_2 \Phi_2 \mathbf{g}_{2k} \mathbf{h}_{1k}, \end{aligned} \quad (20)$$

where $\bar{\mathbf{h}}_k$ has zero mean and variance $\bar{\mathbf{R}}_k = \mathbf{R}_{0k} + \mathbf{R}_{1k} + \mathbf{R}_{2k}$. Its LMMSE estimate is

$$\hat{\bar{\mathbf{h}}}_k = \hat{\mathbf{h}}_k + \hat{\mathbf{h}}_{1k} + \hat{\mathbf{h}}_{2k}, \quad (22)$$

which has zero mean and variance $\bar{\Psi}_k = \Psi_k + \Psi_{1k} + \Psi_{2k}$, while the estimation channel error vector $\bar{\mathbf{e}}_k$ has zero mean and variance $\bar{\mathbf{E}}_k = \mathbf{E}_k + \mathbf{E}_{1k} + \mathbf{E}_{2k}$. In other words, we have

$$\bar{\mathbf{h}}_k = \hat{\bar{\mathbf{h}}}_k + \bar{\mathbf{e}}_k. \quad (23)$$

IV. DOWNLINK ACHIEVABLE RATE

During the downlink data transmission from the BS to UE k in t or r region, the received signal by UE k is expressed based on channel reciprocity as

$$r_k = \bar{\mathbf{h}}_k^H \mathbf{s} + z_k, \quad (24)$$

where $\mathbf{s} = \sqrt{\lambda} \sum_{i=1}^K \sqrt{p_i} \mathbf{f}_i l_i$ denotes the transmit signal vector by the BS. Herein, p_i is the power allocated to UE i , and λ is a constant which is found such that $\mathbb{E}[\mathbf{s}^H \mathbf{s}] = \rho$, where ρ is the total average power budget.⁴ Note that λ is given by $\lambda = \frac{K}{\mathbb{E}\{\text{tr}(\mathbf{F}\mathbf{F}^H)\}}$ to guarantee $\mathbb{E}[\mathbf{s}^H \mathbf{s}] = \rho$, where $\mathbf{F} = [\mathbf{f}_1, \dots, \mathbf{f}_K] \in \mathbb{C}^{M \times K}$. Moreover, $z_k \sim \mathcal{CN}(0, \sigma^2)$ is the additive white complex Gaussian noise at UE k . Also, $\mathbf{f}_i \in \mathbb{C}^{M \times 1}$ is the linear precoding vector and l_i is the corresponding data symbol with $\mathbb{E}\{|l_i|^2\} = 1$.

Taking advantage of the technique in [39] and by exploiting that UEs do not have instantaneous CSI but are aware of only statistical CSI, the downlink SINR can be written as⁵

$$\gamma_k = \frac{S_k}{I_k}, \quad (25)$$

⁴Herein, we rely on a common assumption in the mMIMO literature, which is the adoption of equal power allocation among all UEs, i.e., $p_i = \rho/K$ [32].

⁵We would like to mention that (25) is a known lower bound in the mMIMO literature, which is quite accurate according to the relevant literature, e.g., please see [32], [35]. Apart from this, we have provided Monte-Carlo manipulations in Figs. 2–4 that verify both the correctness and accuracy of the analytical results including this bound.

where

$$S_k = |\mathbb{E}\{\bar{\mathbf{h}}_k^H \mathbf{f}_k\}|^2 \quad (26)$$

$$I_k = \mathbb{E}\left\{|\bar{\mathbf{h}}_k^H \mathbf{f}_k - \mathbb{E}\{\bar{\mathbf{h}}_k^H \mathbf{f}_k\}|^2\right\} + \sum_{i \neq k}^K |\mathbb{E}\{\bar{\mathbf{h}}_k^H \mathbf{f}_i\}|^2 + \frac{K\sigma^2}{\rho\lambda}. \quad (27)$$

Although both maximum ratio transmission (MRT) and regularized zero-forcing (RZF) precoders are common options in the mMIMO literature for the downlink transmission, we select MRT for the sake of simplicity while RZF will be investigated in future work, i.e., $\mathbf{f}_k = \hat{\mathbf{h}}_k$.

The following analysis requires M , N , and K increase but with a given bounded ratio as $0 < \liminf \frac{K}{M} \leq \limsup \frac{K}{M} < \infty$ and $0 < \liminf \frac{N}{M} \leq \limsup \frac{N}{M} < \infty$. Henceforth, this notation is denoted as \asymp . Also, the covariance matrices obey similar assumptions provided in [32, Assump. A1-A3]. Note that the DE analysis allows obtaining deterministic expressions, which makes lengthy Monte-Carlo simulations unnecessary. In parallel, deterministic expressions are tight approximations even for conventional systems with moderate dimensions, e.g., an 8×8 matrix [40].

Proposition 1: The downlink achievable SINR of UE k with MRT precoding for given PBs Φ_1 and Φ_{2,w_k} in a RIS/STAR-RIS assisted mMIMO system, accounting for imperfect CSI and correlated Rayleigh fading, is given by (25), where

$$S_k \asymp \text{tr}^2(\bar{\Psi}_k), \quad (28)$$

$$I_k \asymp \sum_{i=1}^K \text{tr}(\bar{\mathbf{R}}_k \bar{\Psi}_i) - \text{tr}(\bar{\Psi}_k^2) + \frac{K\sigma^2}{\rho} \sum_{i=1}^K \text{tr}(\bar{\Psi}_i). \quad (29)$$

Proof: Please see Appendix B. \blacksquare

The downlink achievable sum SE is given by

$$\text{SE} = \frac{\tau_c - \tau}{\tau_c} \sum_{k=1}^K \log_2(1 + \gamma_k), \quad (30)$$

where the pre-log fraction describes the percentage of samples per coherence block for downlink data transmission.

V. PROBLEM FORMULATION FOR RIS AND STAR-RIS

Based on the common assumption of infinite resolution phase shifters, we propose an alternating optimization algorithm for designing the cooperative reflecting beamforming by optimizing the sum SE with imperfect CSI and correlated fading, which is formulated as

$$\begin{aligned} & \max_{\bar{\boldsymbol{\theta}}, \boldsymbol{\theta}, \boldsymbol{\beta}} \quad \text{SE}(\bar{\boldsymbol{\theta}}, \boldsymbol{\theta}, \boldsymbol{\beta}) \\ & \text{s.t.} \quad |\bar{\theta}_n| = 1, \forall n \in \mathcal{N}_1 \\ & \quad (\beta_n^t)^2 + (\beta_n^r)^2 = 1, \forall n \in \mathcal{N}_2 \\ & \quad \beta_n^t \geq 0, \beta_n^r \geq 0, \forall n \in \mathcal{N}_2 \\ & \quad |\theta_n^t| = |\theta_n^r| = 1, \forall n \in \mathcal{N}_2 \end{aligned} \quad (\mathcal{P}1)$$

where $\boldsymbol{\theta} = [(\boldsymbol{\theta}^t)^\top, (\boldsymbol{\theta}^r)^\top]^\top$ and $\boldsymbol{\beta} = [(\boldsymbol{\beta}^t)^\top, (\boldsymbol{\beta}^r)^\top]^\top$. We have put the variables to be optimized in parentheses to emphasize their presence.

Obviously, the problem ($\mathcal{P}1$) is non-convex. Also, a coupling among the optimization variables appears, which are the phase-shifts of RIS 1 as well as the amplitudes and the phase shifts of the STAR-RIS for transmission and reflection. For the sake of exposition, we define the following three sets describing the feasible set of ($\mathcal{P}1$): $\bar{\Theta} = \{\bar{\boldsymbol{\theta}} \mid |\bar{\theta}_i| = 1, i = 1, 2, \dots, N_1\}$, $\Theta = \{\boldsymbol{\theta} \mid |\theta_i^t| = |\theta_i^r| = 1, i = 1, 2, \dots, N_2\}$, and $\mathcal{B} = \{\boldsymbol{\beta} \mid (\beta_i^t)^2 + (\beta_i^r)^2 = 1, \beta_i^t \geq 0, \beta_i^r \geq 0, i = 1, 2, \dots, N_2\}$. We observe that the project operators of the above sets can be obtained in closed-form, which motivates the application of the PGAM [41, Ch. 2] for the optimization of $\bar{\boldsymbol{\theta}}$, $\boldsymbol{\theta}$, and $\boldsymbol{\beta}$ as follows. In particular, since the optimization problem includes two PBs, which are Φ_1 and Φ_{2,w_k} , we perform alternating optimization by keeping one PB fixed while optimizing the other in an iterative manner until reaching convergence to a stationary point.

Remark 3: Under independent Rayleigh fading conditions and according to Remark 1, the sum rate in (30) is independent of the phase shifts of the RIS and the STAR-RIS, but it can be optimized with respect to the amplitudes of the STAR-RIS.

Thus, we have to apply PGAM two times, one for each surface. Note that each algorithm below achieves a local optimum, i.e., different initializations provide different solutions. In other words, the overall algorithm, based on alternating optimization, results in a local optimum. With this procedure and given the total average power budget constraint regarding (29), the sum-rate increases until convergence.

The proposed algorithms below, i.e., Algorithms 1 and 2 converge quickly and have low computation complexity. Moreover, given that both algorithms achieve a local optimum and that the overall algorithm is based on alternating optimization (AO), the final solution corresponds to a local optimum, which means that different initializations will result in different solutions, as will be shown below in Section VI.

A. Problem Formulation for RIS

The formulation problem for RIS 1 is written as

$$\begin{aligned} & \max_{\bar{\boldsymbol{\theta}}} \quad \text{SE}(\bar{\boldsymbol{\theta}}) \\ & \text{s.t.} \quad |\bar{\theta}_n| = 1, \forall n \in \mathcal{N}_1, \end{aligned} \quad (\mathcal{P}2)$$

where we define the set $\bar{\Theta} = \{\bar{\boldsymbol{\theta}} \mid |\bar{\theta}_i| = 1, i = 1, \dots, N_1\}$.

Given the non-convexity of ($\mathcal{P}2$) in terms of $\bar{\boldsymbol{\theta}}$ and with a unit-modulus constraint regarding $\bar{\theta}_n$, PGAM is a very good candidate as mentioned. Hence, the first PGAM, concerning the RIS, includes the following iteration

$$\bar{\boldsymbol{\theta}}^{n+1} = P_{\bar{\Theta}}(\bar{\boldsymbol{\theta}}^n + \mu_{1,n} \nabla_{\bar{\boldsymbol{\theta}}} \text{SE}(\bar{\boldsymbol{\theta}}^n)). \quad (31)$$

The superscript expresses the iteration count while we move toward the gradient direction to increase the objective. Note that $\mu_{1,n}$ is the step size for $\bar{\boldsymbol{\theta}}$. The difficulty of the problem does not allow to obtain the ideal step size, which should be equal to the inversely proportional of the Lipschitz constant. Thus, to find the step size at each iteration, we apply the Armijo-Goldstein

Algorithm 1: Projected Gradient Ascent Algorithm for RIS
 1 Design.

```

1: Input:  $\bar{\theta}^0, \mu_{1,n} > 0, \kappa_1 \in (0, 1)$ 
2:  $n \leftarrow 1$ 
3: repeat
4:   repeat
5:      $\bar{\theta}^{n+1} = P_{\Theta}(\bar{\theta}^n + \mu_{1,n} \nabla_{\bar{\theta}} \text{SE}(\bar{\theta}^n))$ 
6:     if  $\text{SE}(\bar{\theta}^{n+1}) \leq \bar{Q}_{\mu_{1,n}}(\bar{\theta}^n; \bar{\theta}^{n+1})$  then
7:        $\mu_{1,n} = \mu_{1,n} \kappa_1$ 
8:     end if
9:     until  $\text{SE}(\bar{\theta}^{n+1}) > \bar{Q}_{\mu_{1,n}}(\bar{\theta}^n; \bar{\theta}^{n+1})$ 
10:     $\mu_{1,n+1} \leftarrow \mu_{1,n}$ 
11:     $n \leftarrow n + 1$ 
12:  until convergence
13: Output:  $\bar{\theta}^{n+1}$ 
    
```

backtracking line search by defining a quadratic approximation of $\text{SE}(\bar{\theta})$ as

$$\bar{Q}_{\mu_1}(\bar{\theta}; \mathbf{x}) = \text{SE}(\bar{\theta}) + \langle \nabla_{\bar{\theta}} \text{SE}(\bar{\theta}), \mathbf{x} - \bar{\theta} \rangle - \frac{1}{\mu_1} \|\mathbf{x} - \bar{\theta}\|_2^2. \quad (32)$$

The step size $\mu_{1,n}$ in (31), used at iteration n as the initial step size at iteration $n + 1$, can be obtained as $\mu_{1,n} = L_{1,n} \kappa_1^{m_{1,n}}$, where $L_{1,n} > 0$, $\kappa_1 \in (0, 1)$, and $m_{1,n}$ is the smallest nonnegative integer satisfying

$$\text{SE}(\bar{\theta}^{n+1}) \geq Q_{L_{1,n} \kappa_1^{m_{1,n}}}(\bar{\theta}^n; \bar{\theta}^{n+1}), \quad (33)$$

which is performed by an iterative procedure. The proposed PGAM is described in Algorithm 1.

Proposition 2: The complex gradient $\nabla_{\bar{\theta}} \text{SE}(\bar{\theta})$ is given in closed-form by

$$\nabla_{\bar{\theta}} \text{SE}(\bar{\theta}) = \frac{\tau_c - \tau}{\tau_c \log 2} \sum_{k=1}^K \frac{I_k \nabla_{\bar{\theta}} S_k - S_k \nabla_{\bar{\theta}} I_k}{(1 + \gamma_k) I_k^2}, \quad (34)$$

where

$$\nabla_{\bar{\theta}} S_k = \nu_{0k} \text{diag}(\mathbf{B}_1) + \nu_{1k} \text{diag}(\mathbf{B}_2), \quad (35)$$

$$\nabla_{\bar{\theta}} I_k = \frac{\partial}{\partial \bar{\theta}^*} I_k$$

$$= \text{diag}(\bar{\nu}_{1k} \mathbf{B}_1 + \bar{\nu}_{2k} \mathbf{B}_2 + \sum_{i=1}^K (\tilde{\nu}_{ki1} \mathbf{B}_1 + \tilde{\nu}_{ki2} \mathbf{B}_2)), \quad (36)$$

with $\mathbf{B}_1 = \mathbf{R}_1 \Phi_1 \mathbf{R}_2$, $\mathbf{B}_2 = \mathbf{R}_t \Phi_1 \mathbf{R}_1$, $\nu_{0k} = 2 \text{tr}(\bar{\Psi}_k) \text{tr}(\bar{C} \mathbf{Q}_{0k} \mathbf{R}_{0k} \mathbf{R}_t - \bar{C} \mathbf{Q}_{1k} \mathbf{R}_{0k}^2 \mathbf{Q}_{1k} \mathbf{R}_t + \bar{C} \mathbf{R}_{0k} \mathbf{Q}_{0k} \mathbf{R}_t)$, $\nu_{1k} = 2 \text{tr}(\bar{\Psi}_k) \text{tr}(\hat{\beta}_{1k} \mathbf{Q}_{1k} \mathbf{R}_{1k} \mathbf{R}_1 - \hat{\beta}_{1k} \mathbf{Q}_{1k} \mathbf{R}_{1k}^2 \mathbf{Q}_{1k} \mathbf{R}_1 + \hat{\beta}_{1k} \mathbf{R}_{1k} \mathbf{Q}_{1k} \mathbf{R}_1)$, $\bar{\nu}_{1k} = \bar{C} \text{tr}(\bar{\Psi}_k \mathbf{R}_t)$, $\bar{\nu}_{2k} = \hat{\beta}_{1k} \text{tr}(\bar{\Psi}_k \mathbf{R}_1)$, $\tilde{\nu}_{ki1} = \bar{C} \text{tr}(\bar{\mathbf{R}}_{ki} \mathbf{R}_t)$, and $\tilde{\nu}_{ki2} = \hat{\beta}_{1k} \text{tr}(\bar{\mathbf{R}}_{ki} \mathbf{R}_1)$.

Proof: Please see Appendix C. ■

Note that the projection onto the set $\bar{\Theta}$ for a given $\bar{\theta} \in \mathbb{C}^{2N_1 \times 1}$ is given by

$$P_{\bar{\Theta}}(\bar{\theta}) = \bar{\theta} / |\bar{\theta}| = e^{j \angle \bar{\theta}}. \quad (37)$$

with the operations in the right-hand taking place entry-wise.

B. Problem Formulation for STAR-RIS

In the interesting case of the STAR-RIS, the optimization problem reads as

$$\begin{aligned} \max_{\boldsymbol{\theta}, \boldsymbol{\beta}} \quad & \text{SE}(\boldsymbol{\theta}, \boldsymbol{\beta}) \\ & (\beta_n^t)^2 + (\beta_n^r)^2 = 1, \forall n \in \mathcal{N}_2 \\ & \beta_n^t \geq 0, \beta_n^r \geq 0, \forall n \in \mathcal{N}_2 \\ & |\theta_n^t| = |\theta_n^r| = 1, \forall n \in \mathcal{N}_2, \end{aligned} \quad (\mathcal{P3})$$

where the feasible set of (P3) can be defined for the sake of exposition by the sets $\Theta = \{\boldsymbol{\theta} \mid |\theta_i^t| = |\theta_i^r| = 1, i = 1, 2, \dots, N\}$, and $\mathcal{B} = \{\boldsymbol{\beta} \mid (\beta_i^t)^2 + (\beta_i^r)^2 = 1, \beta_i^t \geq 0, \beta_i^r \geq 0, i = 1, 2, \dots, N\}$. This problem is non-convex, and includes coupling among the amplitudes and the phase shifts for transmission and reflection. Thus, we suggest the application of PGAM, which includes the following iterations

$$\boldsymbol{\theta}^{n+1} = P_{\Theta}(\boldsymbol{\theta}^n + \mu_{2,n} \nabla_{\boldsymbol{\theta}} \text{SE}(\boldsymbol{\theta}^n, \boldsymbol{\beta}^n)), \quad (38a)$$

$$\boldsymbol{\beta}^{n+1} = P_{\mathcal{B}}(\boldsymbol{\beta}^n + \mu_{2,n} \nabla_{\boldsymbol{\beta}} \text{SE}(\boldsymbol{\theta}^n, \boldsymbol{\beta}^n)), \quad (38b)$$

where the step size $\mu_{2,n}$ can be obtained as $\mu_{2,n} = L_{2,n} \kappa_2^{m_{2,n}}$ with $m_{2,n}$ being the smallest nonnegative integer satisfying

$$\text{SE}(\boldsymbol{\theta}^{n+1}, \boldsymbol{\beta}^{n+1}) \geq Q_{L_{2,n} \kappa_2^{m_{2,n}}}(\boldsymbol{\theta}^n, \boldsymbol{\beta}^n; \boldsymbol{\theta}^{n+1}, \boldsymbol{\beta}^{n+1}). \quad (39)$$

Herein, the selection of the step size in (31) and (38a) is crucial for the convergence of the PGAM. Again, we resort to the application of the Armijo-Goldstein backtracking line search to acquire the step size. Hence, we define the quadratic approximation

$$\begin{aligned} Q_{\mu_2}(\boldsymbol{\theta}, \boldsymbol{\beta}; \mathbf{x}, \mathbf{y}) = & \text{SE}(\boldsymbol{\theta}, \boldsymbol{\beta}) + \langle \nabla_{\boldsymbol{\theta}} \text{SE}(\boldsymbol{\theta}, \boldsymbol{\beta}), \mathbf{x} - \boldsymbol{\theta} \rangle \\ & - \frac{1}{\mu_2} \|\mathbf{x} - \boldsymbol{\theta}\|_2^2 + \langle \nabla_{\boldsymbol{\beta}} \text{SE}(\boldsymbol{\theta}, \boldsymbol{\beta}), \mathbf{y} - \boldsymbol{\beta} \rangle \\ & - \frac{1}{\mu_2} \|\mathbf{y} - \boldsymbol{\beta}\|_2^2. \end{aligned} \quad (40)$$

The suggested PGAM is outlined in Algorithm 2.

The description of Algorithm 2 concludes by providing the projection onto the sets Θ and \mathcal{B} . The former is given for a given Θ and \mathcal{B} by the entry-wise operation as

$$P_{\Theta}(\boldsymbol{\theta}) = \boldsymbol{\theta} / |\boldsymbol{\theta}| = e^{j \angle \boldsymbol{\theta}}. \quad (41)$$

In the case of $P_{\mathcal{B}}(\boldsymbol{\beta})$, we observe that the constraint $(\beta_i^t)^2 + (\beta_i^r)^2 = 1, \beta_i^t \geq 0, \beta_i^r \geq 0$ corresponds to the first quadrant of the unit circle, which makes $P_{\mathcal{B}}(\boldsymbol{\beta})$ complicated. To improve the efficiency of $P_{\mathcal{B}}(\boldsymbol{\beta})$ during the iterative process, we allow β_i^t and β_i^r to take negative value without affecting the optimality of the proposed solution, while achieving the same objective. Hence,

Algorithm 2: Projected Gradient Ascent Algorithm for the STAR-RIS Design.

```

1: Input:  $\theta^0, \beta^0, \mu_{2,n} > 0, \kappa_2 \in (0, 1)$ 
2:  $n \leftarrow 1$ 
3: repeat
4:   repeat
5:      $\theta^{n+1} = P_{\Theta}(\theta^n + \mu_{2,n} \nabla_{\theta} \text{SE}(\theta^n, \beta^n))$ 
6:      $\beta^{n+1} = P_B(\beta^n + \mu_{2,n} \nabla_{\beta} \text{SE}(\theta^n, \beta^n))$ 
7:     if  $\text{SE}(\theta^{n+1}, \beta^{n+1}) \leq Q_{\mu_{2,n}}(\theta^n, \beta^n; \theta^{n+1}, \beta^{n+1})$ 
       then
8:        $\mu_{2,n} = \mu_{2,n} \kappa_2$ 
9:     end if
10:    until  $\text{SE}(\theta^{n+1}, \beta^{n+1}) > Q_{\mu_{2,n}}(\theta^n, \beta^n; \theta^{n+1}, \beta^{n+1})$ 
11:     $\mu_{2,n+1} \leftarrow \mu_{2,n}$ 
12:     $n \leftarrow n + 1$ 
13:  until convergence
14: Output:  $\theta^{n+1}, \beta^{n+1}$ 

```

after projecting β_i^t and β_i^r onto the entire unit circle, $P_B(\beta)$ is written as

$$[P_B(\beta)]_i = \frac{\beta_i}{\sqrt{\beta_i^2 + \beta_{i+N}^2}}, i = 1, 2, \dots, N_2 \quad (42a)$$

$$[P_B(\beta)]_{i+N} = \frac{\beta_{i+N}}{\sqrt{\beta_i^2 + \beta_{i+N}^2}}, i = 1, 2, \dots, N_2. \quad (42b)$$

Proposition 3: The complex gradients $\nabla_{\theta} \text{SE}(\theta, \beta)$ and $\nabla_{\beta} \text{SE}(\theta, \beta)$ are obtained in closed-forms by

$$\nabla_{\theta} \text{SE}(\theta, \beta) = [\nabla_{\theta^t} \text{SE}(\theta, \beta)^{\top}, \nabla_{\theta^r} \text{SE}(\theta, \beta)^{\top}]^{\top}, \quad (43a)$$

$$\nabla_{\theta^t} \text{SE}(\theta, \beta) = \frac{\tau_c - \tau}{\tau_c \log 2} \sum_{k=1}^K \frac{I_k \nabla_{\theta^t} S_k - S_k \nabla_{\theta^t} I_k}{(1 + \gamma_k) I_k^2}, \quad (43b)$$

$$\nabla_{\theta^r} \text{SE}(\theta, \beta) = \frac{\tau_c - \tau}{\tau_c \log 2} \sum_{k=1}^K \frac{I_k \nabla_{\theta^r} S_k - S_k \nabla_{\theta^r} I_k}{(1 + \gamma_k) I_k^2}, \quad (43c)$$

where

$$\nabla_{\theta^t} S_k = \begin{cases} \nu_{2k} \text{diag}(\mathbf{B}_{3t} \text{diag}(\beta^t)) \\ + \nu_{3k} \text{diag}(\mathbf{B}_{4t} \text{diag}(\beta^t)) & w_k = t \\ 0 & w_k = r \end{cases} \quad (44a)$$

$$\nabla_{\theta^r} S_k = \begin{cases} \nu_{2k} \text{diag}(\mathbf{B}_{3r} \text{diag}(\beta^r)) \\ + \nu_{3k} \text{diag}(\mathbf{B}_{4r} \text{diag}(\beta^r)) & w_k = r \\ 0 & w_k = t \end{cases} \quad (44b)$$

$$\nabla_{\theta^t} I_k = \text{diag}(\tilde{\mathbf{A}}_{kt} \text{diag}(\beta^t)) \quad (44c)$$

$$\nabla_{\theta^r} I_k = \text{diag}(\tilde{\mathbf{A}}_{kr} \text{diag}(\beta^r)) \quad (44d)$$

with

$$\tilde{\mathbf{A}}_{kt} = \begin{cases} \tilde{\nu}_{2k} \mathbf{B}_3 + \tilde{\nu}_{2k} \mathbf{B}_4 + \sum_{i \in \mathcal{K}_t} (\tilde{\nu}_{ki2} \mathbf{B}_3 + \tilde{\nu}_{ki2} \mathbf{B}_4) & w_k = t \\ \sum_{i \in \mathcal{K}_t} (\tilde{\nu}_{ki2} \mathbf{B}_3 + \tilde{\nu}_{ki2} \mathbf{B}_4) & w_k \neq t \end{cases} \quad (45)$$

with $\mathbf{B}_{3t} = \mathbf{R}_1 \Phi_{2,t} \mathbf{R}_2$, $\bar{\mathbf{D}} = \text{tr}(\mathbf{B}_1 \Phi_1^{\text{H}}) \mathbf{R}_t$, $\mathbf{B}_{4t} = \hat{\beta}_{2k} \text{tr}(\mathbf{R}_t \Phi_{2,t} \mathbf{R}_2)$ for $w_k \in \{t, r\}$, $\nu_{2k} = 2 \text{tr}(\tilde{\Psi}_k) \text{tr}(\mathbf{Q}_{0k} \mathbf{R}_{0k} \bar{\mathbf{D}} - \mathbf{Q}_{1k} \mathbf{R}_{0k}^2 \mathbf{Q}_{1k} \bar{\mathbf{D}} + \mathbf{R}_{0k} \mathbf{Q}_{0k} \bar{\mathbf{D}})$, $\nu_{3k} = 2 \text{tr}(\tilde{\Psi}_k) \text{tr}(\mathbf{Q}_{2k} \mathbf{R}_{2k} \mathbf{R}_2 - \mathbf{Q}_{2k} \mathbf{R}_{2k}^2 \mathbf{Q}_{2k} \mathbf{R}_2 + \mathbf{R}_{2k} \mathbf{Q}_{2k} \mathbf{R}_2)$, $\tilde{\nu}_{1k} = \text{tr}(\tilde{\Psi}_k \bar{\mathbf{D}})$, $\tilde{\nu}_{2k} = \hat{\beta}_{1k} \text{tr}(\tilde{\Psi}_k \mathbf{R}_2)$, $\tilde{\nu}_{ki1} = \text{tr}(\tilde{\mathbf{R}}_{ki} \bar{\mathbf{D}})$, and $\tilde{\nu}_{ki2} = \hat{\beta}_{1k} \text{tr}(\tilde{\mathbf{R}}_{ki} \mathbf{R}_2)$. In a similar way, the real-valued gradient $\nabla_{\beta} \text{SE}(\theta, \beta)$ is given by

$$\nabla_{\beta} \text{SE}(\theta, \beta) = [\nabla_{\beta^t} \text{SE}(\theta, \beta)^{\top}, \nabla_{\beta^r} \text{SE}(\theta, \beta)^{\top}]^{\top}, \quad (46a)$$

$$\nabla_{\beta^t} \text{SE}(\theta, \beta) = \frac{\tau_c - \tau}{\tau_c \log 2} \sum_{k=1}^K \frac{I_k \nabla_{\beta^t} S_k - S_k \nabla_{\beta^t} I_k}{(1 + \gamma_k) I_k^2}, \quad (46b)$$

$$\nabla_{\beta^r} \text{SE}(\theta, \beta) = \frac{\tau_c - \tau}{\tau_c \log 2} \sum_{k=1}^K \frac{I_k \nabla_{\beta^r} S_k - S_k \nabla_{\beta^r} I_k}{(1 + \gamma_k) I_k^2}, \quad (46c)$$

where

$$\nabla_{\beta^t} S_k = \begin{cases} 2 \text{Re}\{\bar{\mathbf{D}}(\text{diag}(\mathbf{B}_{3t}^{\text{H}} \text{diag}(\beta^t)))\} \\ + 2 \text{Re}\{\mathbf{R}_2(\text{diag}(\mathbf{B}_{4t}^{\text{H}} \text{diag}(\beta^t)))\} & w_k = t \\ 0 & w_k = r \end{cases} \quad (47a)$$

$$\nabla_{\beta^r} S_k = \begin{cases} 2 \text{Re}\{\bar{\mathbf{D}}(\text{diag}(\mathbf{B}_{3r}^{\text{H}} \text{diag}(\beta^r)))\} \\ + 2 \text{Re}\{\mathbf{R}_2(\text{diag}(\mathbf{B}_{4r}^{\text{H}} \text{diag}(\beta^r)))\} & w_k = r \\ 0 & w_k = t, \end{cases} \quad (47b)$$

$$\nabla_{\theta^t} I_k = 2 \text{Re}\{\text{diag}(\tilde{\mathbf{A}}_{kt} \text{diag}(\beta^t))\} \quad (47c)$$

$$\nabla_{\theta^r} I_k = 2 \text{Re}\{\text{diag}(\tilde{\mathbf{A}}_{kr} \text{diag}(\beta^r))\}. \quad (47d)$$

Proof: Please see Appendix D. \blacksquare

As mentioned, under independent Rayleigh fading conditions, which are unrealistic in practice, Algorithm 1 would not execute because no dependence on the phase shifts appears. Similarly, Algorithm 2 would execute only with respect to the amplitudes of STAR-RIS.

Remark 4: We have optimized the amplitude and phase shift, separately, rather than optimizing them as a single complex although the presentation of the proposed method would be more elegant if we had chosen one variable for both of them. However, despite that extensive numerical experiments revealed that both ways give the same performance in many cases, in some cases, the use of two separate variables yields a better performance. Hence, this numerical observation has lead to the separate independent optimization of the amplitudes and phase shifts.

C. Complexity Analysis of Algorithms 1 and 2

Herein, we provide the complexity analysis for each iteration of Algorithm 1. Regarding \mathbf{R}_{0k} , \mathbf{R}_{1k} , \mathbf{R}_{2k} , the traces

require $\mathcal{O}(N^2)$ complex multiplications because Φ_1 is diagonal, while their overall expression requires in total $\mathcal{O}(M^3 + N^2)$ complex multiplications since the trace is multiplied with a $M \times M$ matrix. Also, Ψ_k , including a matrix inversion, takes $\mathcal{O}(M^3)$ complex multiplications, which could be reduced by applying eigenvalue decomposition (EVD). Thus, SE requires $\mathcal{O}(K(N^2 + M^3))$ iterations. The same number of iterations is required by $\nabla_{\hat{\theta}} \text{SE}(\hat{\theta})$. The complexity of Algorithm 2 can be shown that is the same by following the same steps.

Convergence Analysis of Algorithm 2: We follow standard arguments for projected gradient methods to show the convergence of Algorithm 2. First, the gradients $\nabla_{\theta} f(\theta, \beta)$ and $\nabla_{\beta} f(\theta, \beta)$ are Lipschitz continuous⁶ over the feasible set since they comprise basic functions. If we denote L_{θ} and L_{β} the Lipschitz constant of $\nabla_{\theta} f(\theta, \beta)$ and $\nabla_{\beta} f(\theta, \beta)$, respectively, we have that [41, Chapter 2]

$$\begin{aligned} f(\mathbf{x}, \mathbf{y}) &\geq f(\theta, \beta) + \langle \nabla_{\theta} f(\theta, \beta), \mathbf{x} - \theta \rangle - \frac{1}{L_{\theta}} \|\mathbf{x} - \theta\|_2^2 \\ &\quad + \langle \nabla_{\beta} f(\theta, \beta), \mathbf{y} - \beta \rangle - \frac{1}{L_{\beta}} \|\mathbf{y} - \beta\|_2^2 \\ &\geq f(\theta, \beta) + \langle \nabla_{\theta} f(\theta, \beta), \mathbf{x} - \theta \rangle - \frac{1}{L_{\max}} \|\mathbf{x} - \theta\|_2^2 \\ &\quad + \langle \nabla_{\beta} f(\theta, \beta), \mathbf{y} - \beta \rangle - \frac{1}{L_{\max}} \|\mathbf{y} - \beta\|_2^2 \quad (48) \end{aligned}$$

where $L_{\max} = \max(L_{\theta}, L_{\beta})$. Hence, the termination of the line search procedure of Algorithm 2 is achieved in finite iterations because the condition in Step 10 must be satisfied when $\mu_n < L_{\max}$. In particular, given μ_{n-1} , the maximum number of steps in the line search procedure is $\left\lceil \frac{\log(L_{\max} \mu_{n-1})}{\log \kappa} \right\rceil$, where $\log(\cdot)$ denotes the natural logarithm and $\lceil \cdot \rceil$ denotes the smallest integer that is larger than or equal to the argument. Moreover, because of the line search, we automatically obtain an increasing sequence of objectives, i.e., $f(\theta^{n+1}, \beta^{n+1}) \geq f(\theta^n, \beta^n)$. Given that the feasible sets Θ and \mathcal{B} are compact, $f(\theta^n, \beta^n)$ must converge. Notably, L_{θ} and L_{β} are not required to run Algorithm 2.

VI. NUMERICAL RESULTS

In this section, we discuss the numerical results corresponding to the downlink sum SE of double RIS-assisted mMIMO systems under correlated Rayleigh fading conditions. MC simulations corroborate our analysis even for finite (conventional) system dimensions, which agrees with a similar observation in [32], [40], [42].

The simulation setup consists of a conventional RIS and a STAR that facilitate the communication between an mMIMO BS, which serves $K = 4$ UEs. Both surfaces are formed by a UPA of $N = 64$ elements with each having dimensions $d_H = d_V = \lambda/4$, while the BS is formed by a uniform linear array (ULA) of $M = 64$ antennas. The 3D spatial locations of the network nodes being the BS, conventional RIS, and STAR-RIS are given as $(x_B, y_B, z_B) = (0, 0, 0)$, $(x_R, y_R, z_R) =$

⁶A function $\mathbf{h}(\mathbf{x})$ is Lipschitz continuous over the set D if there exists $L > 0$ such that $\|\mathbf{h}(\mathbf{x}) - \mathbf{h}(\mathbf{y})\| \leq L\|\mathbf{x} - \mathbf{y}\|_2$.

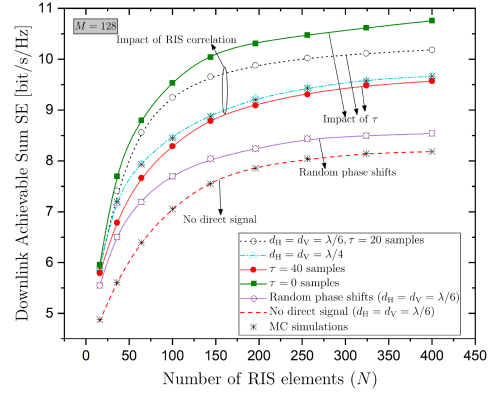


Fig. 2. Downlink achievable sum SE versus the total number of RIS elements N of a RIS/STAR-RIS assisted mMIMO system with imperfect CSI ($M = 100$, $K = 4$) for varying conditions (Analytical results and MC simulations).

(50, 10, 20), and $(x_{SR}, y_{SR}, z_{SR}) = (100, 30, 20)$ respectively, all in meter units. Regarding the UEs in the r region, they are located on a straight line between $(x_{SR} - \frac{1}{2}d_0, y_{SR} - \frac{1}{2}d_0)$ and $(x_{SR} + \frac{1}{2}d_0, y_{SR} - \frac{1}{2}d_0)$ with equal distances between each two adjacent users, and $d_0 = 20$ m in our simulations. UEs in the t region are located between $(x_{SR} - \frac{1}{2}d_0, y_{SR} + \frac{1}{2}d_0)$ and $(x_{SR} + \frac{1}{2}d_0, y_{SR} + \frac{1}{2}d_0)$. In this work, we consider distance-based path-loss, where the channel gain of a given link j is $\tilde{\beta}_j = Ad_j^{-\alpha_j}$ with the channel gain of a given link j being $\tilde{\beta}_j = Ad_j^{-\alpha_j}$. The variables A and α_j denote the area of each reflecting element at the RIS and the path-loss exponent, respectively. The path losses $\tilde{\beta}_j$, $\tilde{\beta}_g$, and $\tilde{\beta}_k$ are assumed to have the same values but the latter is assumed to have a further penetration loss equal to 15 dB. The correlation matrices \mathbf{R}_{BS} and \mathbf{R}_{RIS} are evaluated based on [30] and [32], respectively. We assume that both surfaces have the same correlation. The variance of the noise is $\sigma^2 = -174 + 10 \log_{10} B_c$, where $B_c = 200$ kHz is the bandwidth. The coherence time is $T_c = 1$ ms, i.e., each coherence block consists of $\tau_c = 200$ samples, and we assume that the duration of the channel estimation phase is $\tau = 20$ samples.

As baseline schemes, we consider the conventional double-RIS, where the STAR-RIS is replaced by a conventional surface split into two subsurfaces that consist of transmitting-only and reflecting-only elements, each with N_{2t} and N_{2r} elements, such that $N_{2t} + N_{2r} = N_2$. Also, we consider the single-RIS counterparts, which consist of a single STAR-RIS with $N = N_1 + N_2$ elements, or a single conventional RIS with the same number of elements.

Fig. 2 depicts the achievable sum SE versus the total number of RIS elements $N = N_1 + N_2$ by studying the effect of spatial correlation while changing the size of each RIS element. Obviously, the downlink sum SE increases with N as expected. Regarding the effect of spatial correlation, it is shown that the performance increases as the correlation decreases by increasing the size of the RIS elements. In addition, we have depicted the scenario of random phase shifts, i.e., no optimization has taken place on any of the surfaces. Hence, the performance is lower

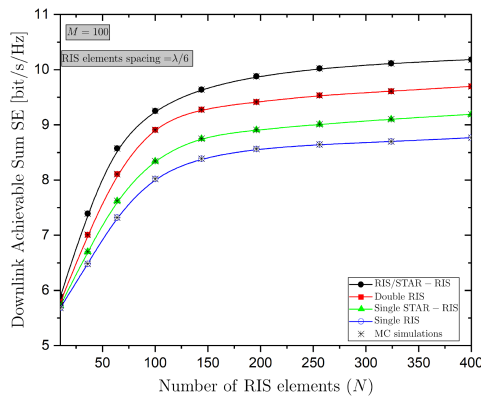


Fig. 3. Downlink achievable sum SE versus the total number of RIS elements N of a RIS/STAR-RIS assisted mMIMO system with imperfect CSI ($M = 100$, $K = 4$) for different architectures (Analytical results and MC simulations).

than in the case of optimized RISs. Also, we have provided the performance of no direct signal, which shows that the surfaces contribute to the sum-rate. In the same figure, we have depicted the impact of imperfect CSI by varying τ , which expresses the duration of the channel estimation phase. In particular, the case $\tau = 0$ corresponds to the perfect CSI scenario, which presents the best performance. The case, where $\tau = 20$ samples presents lower performance, while by increasing τ to 40 samples, the performance worsens even more.

Fig. 3 demonstrates the superiority of the proposed combination of RIS with a STAR-RIS in terms of the achievable sum SE versus the total number of RIS elements N . Specifically, we observe that the RIS/STAR-RIS outperforms the conventional double-RIS design including the double and single reflected links. The reason is the introduction of the advantageous STAR-RIS, which exploits more degrees of freedom with respect to a conventional reflecting-only RIS. In comparison to single-RIS counterparts, the double-RIS design enjoys the cooperative PB gain, and additionally, to this, the proposed model outperforms the conventional single RIS due to the presence of more adjustable (reflection and transmission) parameters.

Figs. 4 illustrates the achievable sum SE versus the number of BS antennas M for different architectures being the RIS/STAR-RIS, double-RIS, single STAR-RIS, and single RIS. Apart from the fact that the sum SE increases with M in all cases. In particular, we observe that when two RIS are deployed but the second surface is a STAR-RIS, the sum SE is higher. In the case of a single RIS, despite the type of the surface, which can be a conventional RIS or a STAR-RIS, the performance is lower than having two RISs as expected because this scenario does not enjoy the double-RIS PB gain. In all cases, which include a STAR-RIS, the performance is better than the reflective only counterpart since both the transmission and reflection coefficients of each element can be optimized.

Fig. 5 shows the achievable sum SE versus the SNR for different layouts as in Fig. 3. The RIS/STAR-RIS implementation presents the best performance by exploiting its STAR-RIS part, which brings a higher degree of flexibility by optimizing both the transmission and reflection coefficients of each element. On

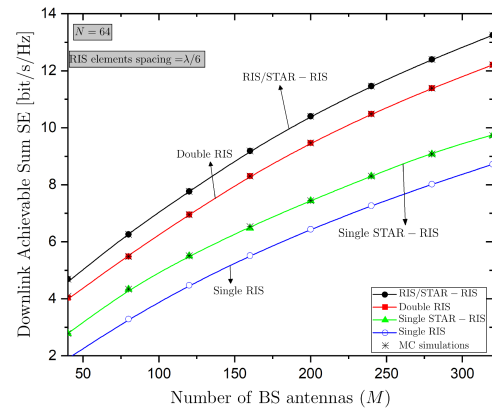


Fig. 4. Downlink achievable sum SE versus the number of BS antennas M of a RIS/STAR-RIS assisted mMIMO system with imperfect CSI for $N = 64$, $K = 4$ under varying conditions (Analytical results).

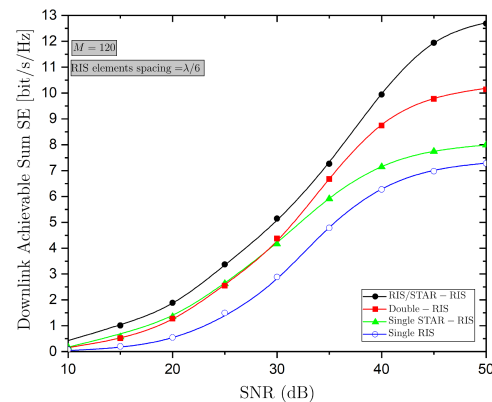


Fig. 5. Downlink achievable sum SE versus the SNR of a RIS/STAR-RIS assisted mMIMO system with imperfect CSI ($M = 100$, $N = 64$, $K = 4$) for varying conditions (Analytical results).

the contrary, in the case of conventional RIS, only one type of the coefficients can be optimized each time, i.e., the transmission or the reflection coefficient. Also, the RIS/STAR-RIS and double RIS layouts, which include two surfaces, benefit from the double-RIS PB gain.

Fig. 6 illustrates the achievable sum SE versus the number of elements N_1 of surface 1, i.e., the conventional RIS given the total number of elements $N = N_1 + N_2 = 320$. For the sake of reference, we have depicted the scenarios of double-RIS, single RIS, and STAR/RIS. In other words, we have shown the scenarios with 2 surfaces and their single-surface counterparts. The former always achieve better rate performance compared to the single RIS baselines. Also, the the RIS/STAR-RIS model performs better than the reflective-only double-RIS model. Moreover, we observe that the rate is maximized when the 2 surfaces have almost equal number of elements.

Fig. 7 elaborates on the convergence of the proposed projected gradient algorithm for the STAR-RIS. Given that 1 and 2 have similar structures but 1 is simpler, similar observations concern it. In particular, in the case of 2, we depict the achievable sum SE against the iteration count returned for 5 different randomly

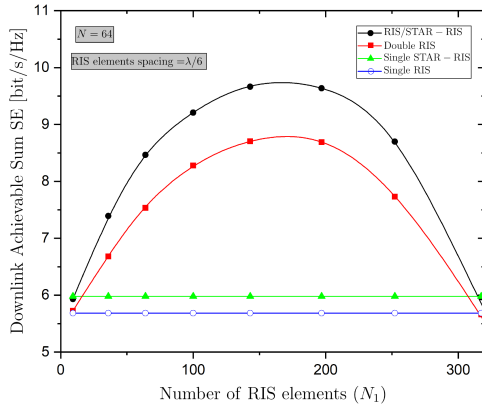


Fig. 6. Downlink achievable sum SE versus the SNR of a RIS/STAR-RIS assisted mMIMO system with imperfect CSI ($M = 100$, $N = 64$, $K = 4$) for varying conditions (Analytical results).

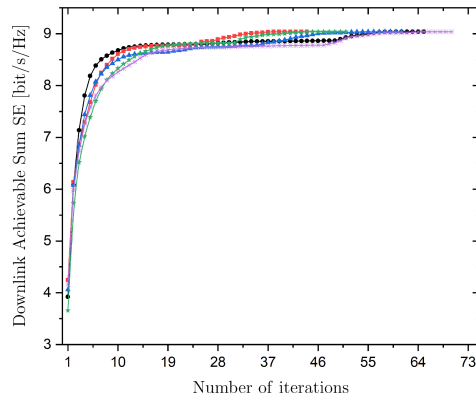


Fig. 7. Convergence of Algorithm 2 for a RIS/STAR-RIS assisted mMIMO system with imperfect CSI ($M = 100$, $N = 64$, $K = 4$).

generated initial points. By assuming equal power splitting between transmission and reception mode, the initial values for β_r and β_t are $\sqrt{0.5}$. The initial values for θ_r and θ_t are drawn from the Uniform distribution over $[0, 2\pi]$. The algorithm terminates when the increase of the objective between the two last iterations is less than 10^{-5} or the number of iterations is larger than 200. Since the problem is nonconvex, Algorithm 2 provides a not necessarily optimal solution. Hence, Algorithm 2 may start from different initial points and lead to different points with different convergence rates. To address this sensitivity issue, we run Algorithm 2 from different initial points and select the best convergent solutions, simulations have shown that to achieve a good trade-off between complexity and achievable sum SE, a good option option is to run 2 from 5 randomly generated initial points.

VII. CONCLUSION

In this paper, we proposed a RIS/STAR-RIS assisted mMIMO communication system by exploiting the cooperative beamforming and full coverage under correlated Rayleigh fading conditions and the coexistence of both double and single links. Moreover, we obtained the estimated channels and derived the DE of the sum SE in closed form in terms of large-scale statistics, which induce low overhead. Next, we formulated and solved the

cooperative beamforming optimization problem to maximise the sum SE. The closed-form gradients came with low complexity and reduced overhead which is crucial, especially, in STAR-RIS architectures that include double parameters. One of the two main reasons for reduced overhead during optimization is that it can be performed at every several coherence intervals. The other reason is that we optimized the amplitudes and phase shifts of the STAR-RIS simultaneously. Simulation results showed substantial performance improvement compared to conventional double RIS or single RIS counterparts. As a future work, the study of more general multi-RIS architectures with more than two hops for reflection and transmission could be investigated to reach the full potential of a smart wireless environment.

APPENDIX A

PROOF OF LEMMA 1

The LMMSE estimator of \mathbf{h}_k results from the minimization of $\text{tr}(\mathbb{E}\{(\hat{\mathbf{h}}_k - \mathbf{h}_k)(\hat{\mathbf{h}}_k - \mathbf{h}_k)^H\})$, which gives

$$\hat{\mathbf{h}}_k = \mathbb{E}\{\mathbf{r}_k \mathbf{h}_k^H\} (\mathbb{E}\{\mathbf{r}_k \mathbf{r}_k^H\})^{-1} \mathbf{r}_k. \quad (49)$$

The first expectation is obtained by exploiting that the channel and the receiver noise are uncorrelated. In particular, we have

$$\mathbb{E}\{\mathbf{r}_k \mathbf{h}_k^H\} = \mathbb{E}\{\mathbf{h}_k \mathbf{h}_k^H\} = \mathbf{R}_{0k}. \quad (50)$$

The second term in (49) is obtained as

$$\mathbb{E}\{\mathbf{r}_k \mathbf{r}_k^H\} = \mathbf{R}_{0k} + \frac{\sigma^2}{\tau P} \mathbf{I}_M. \quad (51)$$

The LMMSE estimate in (17) is obtained by substituting (50) and (51) into (49). Also, the covariance matrix of the estimated channel is obtained as

$$\mathbb{E}\{\hat{\mathbf{h}}_k \hat{\mathbf{h}}_k^H\} = \mathbf{R}_{0k} \mathbf{Q}_{0k} \mathbf{R}_{0k}. \quad (52)$$

APPENDIX B

PROOF OF PROPOSITION 1

The DE of S_k in (26) can be written as

$$S_k = |\mathbb{E}\{\bar{\mathbf{h}}_k^H \hat{\mathbf{h}}_k\}|^2 \asymp |\mathbb{E}\{\hat{\mathbf{h}}_k^H \hat{\mathbf{h}}_k\}|^2 \quad (53)$$

$$= |\text{tr}(\bar{\Psi}_k)|^2, \quad (54)$$

where, in (53), we have taken into account the independence between the channel and its estimated version. The last equation is obtained based on [42, Lem. 4].

Regarding the first term of I_k in (27), we have

$$\mathbb{E}\left\{ \left| \bar{\mathbf{h}}_k^H \hat{\mathbf{h}}_k - \mathbb{E}\left\{ \bar{\mathbf{h}}_k^H \hat{\mathbf{h}}_k \right\} \right|^2 \right\} = \mathbb{E}\left\{ \left| \bar{\mathbf{h}}_k^H \hat{\mathbf{h}}_k \right|^2 \right\} - \left| \mathbb{E}\left\{ \bar{\mathbf{h}}_k^H \hat{\mathbf{h}}_k \right\} \right|^2 \quad (55)$$

$$\asymp \mathbb{E}\left\{ \left| \hat{\mathbf{h}}_k^H \hat{\mathbf{h}}_k + |\bar{\mathbf{e}}_k^H \hat{\mathbf{h}}_k|^2 \right\} \right\} - \left| \mathbb{E}\left\{ \hat{\mathbf{h}}_k^H \hat{\mathbf{h}}_k \right\} \right|^2 \quad (56)$$

$$= \mathbb{E}\left\{ |\bar{\mathbf{e}}_k^H \hat{\mathbf{h}}_k|^2 \right\} \quad (57)$$

$$\asymp \text{tr}(\bar{\mathbf{R}}_k \bar{\Psi}_k) - \text{tr}(\bar{\Psi}_k^2), \quad (58)$$

where in (56), we have used (23), and that $\mathbb{E}\{|X + Y|^2\} = \mathbb{E}\{|X|^2\} + \mathbb{E}\{|Y|^2\}$, which is valid for any two uncorrelated

random variables while one of them has zero mean value. The last equation is derived by taking into account the uncorrelation between the two random vectors and by application of [42, Lem. 4].

The second term of I_k in (27) is obtained as

$$\mathbb{E} \left\{ |\bar{\mathbf{h}}_k^H \hat{\mathbf{h}}_i|^2 \right\} \asymp \text{tr}(\bar{\mathbf{R}}_k \bar{\Psi}_i) \quad (59)$$

due to the uncorrelation between \mathbf{h}_k and $\hat{\mathbf{h}}_i$ and [42, Lem. 4]. The normalization parameter is obtained as

$$\lambda = \frac{1}{\sum_{i=1}^K \mathbb{E}\{\mathbf{f}_i^H \mathbf{f}_i\}} = \frac{1}{\sum_{i=1}^K \mathbb{E}\{\hat{\mathbf{h}}_i^H \hat{\mathbf{h}}_i\}} \asymp \frac{1}{\sum_{i=1}^K \text{tr}(\bar{\Psi}_i)}. \quad (60)$$

The proof concludes by inserting (54), (58), (59), and (60) into (26) and (27).

APPENDIX C PROOF OF PROPOSITION 2

Based on (30), we can easily obtain

$$\nabla_{\bar{\theta}} \text{SE}(\bar{\theta}) = \frac{\tau_c - \tau}{\tau_c \log 2} \sum_{k=1}^K \frac{I_k \nabla_{\bar{\theta}} S_k - S_k \nabla_{\bar{\theta}} I_k}{(1 + \gamma_k) I_k^2}. \quad (61)$$

For the derivation of $\nabla_{\bar{\theta}} S_k$ with fixed Φ_{2,w_k} , we derive its differential as

$$\begin{aligned} d(S_k) &= d(\text{tr}(\bar{\Psi}_k)^2) \\ &= 2\text{tr}(\bar{\Psi}_k) d\text{tr}(\bar{\Psi}_k) \\ &= 2\text{tr}(\bar{\Psi}_k) \text{tr}(d(\bar{\Psi}_k)). \end{aligned} \quad (62)$$

The next step concerns the derivation of $d(\Psi_k)$. First, we write $\bar{\Psi}_k$ as

$$\bar{\Psi}_k = \Psi_k + \Psi_{1k} + \Psi_2 \quad (63)$$

$$= \mathbf{R}_{0k} \mathbf{Q}_{0k} \mathbf{R}_{0k} + \mathbf{R}_{1k} \mathbf{Q}_{1k} \mathbf{R}_{1k} + \mathbf{R}_{2k} \mathbf{Q}_{2k} \mathbf{R}_{2k}. \quad (64)$$

By using [43, Eq. (3.35)], its differential becomes

$$\begin{aligned} d(\bar{\Psi}_k) &= d(\mathbf{R}_{0k}) \mathbf{Q}_{0k} \mathbf{R}_{0k} + \mathbf{R}_{0k} d(\mathbf{Q}_{0k}) \mathbf{R}_{0k} \\ &\quad + \mathbf{R}_{0k} \mathbf{Q}_{0k} d(\mathbf{R}_{0k}) + d(\mathbf{R}_{1k}) \mathbf{Q}_{1k} \mathbf{R}_{1k} \\ &\quad + \mathbf{R}_{1k} d(\mathbf{Q}_{1k}) \mathbf{R}_{1k} + \mathbf{R}_{1k} \mathbf{Q}_{1k} d(\mathbf{R}_{1k}) \end{aligned} \quad (65)$$

since \mathbf{R}_{2k} and \mathbf{Q}_{2k} do not depend on Φ_1 .

Regarding $d(\mathbf{Q}_{0k})$, use of [43, eqn. (3.40)] gives

$$\begin{aligned} d(\mathbf{Q}_{0k}) &= d\left(\mathbf{R}_{0k} + \frac{\sigma}{\tau P} \mathbf{I}_M\right)^{-1} \\ &= -\left(\mathbf{R}_{0k} + \frac{\sigma^2}{\tau P} \mathbf{I}_M\right)^{-1} d\left(\mathbf{R}_{0k} + \frac{\sigma^2}{\tau P} \mathbf{I}_M\right) \\ &\quad \times \left(\mathbf{R}_{0k} + \frac{\sigma}{\tau P} \mathbf{I}_M\right)^{-1} \\ &= -\mathbf{Q}_{0k} d(\mathbf{R}_{0k}) \mathbf{Q}_{0k}. \end{aligned} \quad (66)$$

Similarly, we obtain

$$d(\mathbf{Q}_{1k}) = -\mathbf{Q}_{1k} d(\mathbf{R}_{1k}) \mathbf{Q}_{1k}. \quad (67)$$

Inserting (66) and (67) into (65), it yields

$$\begin{aligned} d(\Psi_k) &= d(\mathbf{R}_{0k}) \mathbf{Q}_{0k} \mathbf{R}_{0k} - \mathbf{R}_{0k} \mathbf{Q}_{1k} d(\mathbf{R}_{1k}) \mathbf{Q}_{1k} \mathbf{R}_{0k} \\ &\quad + \mathbf{R}_{0k} \mathbf{Q}_{0k} d(\mathbf{R}_{0k}) + d(\mathbf{R}_{1k}) \mathbf{Q}_{1k} \mathbf{R}_{1k} \\ &\quad - \mathbf{R}_{1k} \mathbf{Q}_{1k} d(\mathbf{R}_{1k}) \mathbf{Q}_{1k} \mathbf{R}_{1k} + \mathbf{R}_{1k} \mathbf{Q}_{1k} d(\mathbf{R}_{1k}). \end{aligned} \quad (68)$$

Now, we have to obtain $d(\mathbf{R}_{0k})$ and $d(\mathbf{R}_{1k})$ given that $\mathbf{R}_{0k} = \hat{\beta}_k \text{tr}(\mathbf{R}_1 \Phi_{2,w_k} \mathbf{R}_2 \Phi_{2,w_k}^H) \text{tr}(\mathbf{B}_1 \Phi_1^H) \mathbf{R}_t$ and $\mathbf{R}_{1k} = \hat{\beta}_{1k} \text{tr}(\mathbf{B}_2 \Phi_1^H) \mathbf{R}_1$, where $\mathbf{B}_1 = \mathbf{R}_1 \Phi_1 \mathbf{R}_2$ and $\mathbf{B}_2 = \mathbf{R}_t \Phi_1 \mathbf{R}_1$. First, we write $d(\mathbf{R}_{0k})$ as

$$\begin{aligned} d(\mathbf{R}_{0k}) &= \bar{C} \text{tr}(\mathbf{B}_1^H \Phi_1 + \mathbf{B}_1 d(\Phi_1^H)) \mathbf{R}_t \\ &= \bar{C} \mathbf{R}_t \left((\text{diag}(\mathbf{B}_1^H))^T d(\bar{\theta}) + (\text{diag}(\mathbf{B}_1))^T d(\bar{\theta}^*) \right), \end{aligned} \quad (69)$$

where $\bar{C} = \hat{\beta}_k \text{tr}(\mathbf{R}_1 \Phi_{2,w_k} \mathbf{R}_2 \Phi_{2,w_k}^H)$, while the last equation is obtained by exploiting that Φ_1 is diagonal.

Similarly, we have

$$\begin{aligned} d(\mathbf{R}_{1k}) &= \hat{\beta}_{1k} \text{tr}(\mathbf{B}_2^H d(\Phi_1) + \mathbf{B}_2 d(\Phi_1)) \mathbf{R}_1 \\ &= \hat{\beta}_{1k} \mathbf{R}_1 \left((\text{diag}(\mathbf{B}_2^H))^T d(\bar{\theta}) + (\text{diag}(\mathbf{B}_2))^T d(\bar{\theta}^*) \right). \end{aligned} \quad (70)$$

Substitution of (68) into (62) results in

$$\begin{aligned} d(S_k) &= 2\text{tr}(\bar{\Psi}_k) \text{tr}(\mathbf{Q}_{0k} \mathbf{R}_{0k} d(\mathbf{R}_{0k}) - \mathbf{Q}_{1k} \mathbf{R}_{0k}^2 \mathbf{Q}_{1k} d(\mathbf{R}_{0k}) \\ &\quad + \mathbf{R}_{0k} \mathbf{Q}_{0k} d(\mathbf{R}_{0k}) + \mathbf{Q}_{1k} \mathbf{R}_{1k} d(\mathbf{R}_{1k}) \\ &\quad - \mathbf{Q}_{1k} \mathbf{R}_{1k}^2 \mathbf{Q}_{1k} d(\mathbf{R}_{1k}) \mathbf{R}_{1k} \mathbf{Q}_{1k} d(\mathbf{R}_{1k})) \\ &= \nu_{0k} \left((\text{diag}(\mathbf{B}_1^H))^T d(\bar{\theta}) + (\text{diag}(\mathbf{B}_1))^T d(\bar{\theta}^*) \right) \\ &\quad + \nu_{1k} \left((\text{diag}(\mathbf{B}_2^H))^T d(\bar{\theta}) + (\text{diag}(\mathbf{B}_2))^T d(\bar{\theta}^*) \right) \end{aligned} \quad (71)$$

where

$$\begin{aligned} \nu_{0k} &= 2\text{tr}(\bar{\Psi}_k) \text{tr}(\bar{C} \mathbf{Q}_{0k} \mathbf{R}_{0k} \mathbf{R}_t - \bar{C} \mathbf{Q}_{1k} \mathbf{R}_{0k}^2 \mathbf{Q}_{1k} \mathbf{R}_t \\ &\quad + \bar{C} \mathbf{R}_{0k} \mathbf{Q}_{0k} \mathbf{R}_t), \end{aligned} \quad (72)$$

$$\begin{aligned} \nu_{1k} &= 2\text{tr}(\bar{\Psi}_k) \text{tr}(\hat{\beta}_{1k} \mathbf{Q}_{1k} \mathbf{R}_{1k} \mathbf{R}_1 - \hat{\beta}_{1k} \mathbf{Q}_{1k} \mathbf{R}_{1k}^2 \mathbf{Q}_{1k} \mathbf{R}_1 \\ &\quad + \hat{\beta}_{1k} \mathbf{R}_{1k} \mathbf{Q}_{1k} \mathbf{R}_1). \end{aligned} \quad (73)$$

Note that in (74), we have inserted (70) and (72).

From (74), we obtain that

$$\begin{aligned} \nabla_{\bar{\theta}} S_k &= \frac{\partial}{\partial \bar{\theta}} S_k \\ &= \nu_{0k} \text{diag}(\mathbf{B}_1) + \nu_{1k} \text{diag}(\mathbf{B}_2), \end{aligned} \quad (74)$$

which proves (35).

In the case of $\nabla_{\bar{\theta}} I_k$, we focus on the differential of I_k

$$\begin{aligned} d(I_k) &= \sum_{i=1}^K \text{tr}(d(\bar{\mathbf{R}}_k) \bar{\Psi}_i) + \sum_{i=1}^K \text{tr}(\mathbf{R}_k d(\bar{\Psi}_i)) \\ &\quad - 2\text{tr}(\bar{\Psi}_k d(\bar{\Psi}_k)) + \frac{K\sigma^2}{\rho} \sum_{i=1}^K \text{tr}(d(\bar{\Psi}_i)) \end{aligned} \quad (75)$$

$$= \text{tr}(\tilde{\Psi}d(\bar{\mathbf{R}}_k)) - 2\text{tr}(\bar{\Psi}_k d(\bar{\Psi}_k)) + \sum_{i=1}^K \text{tr}(\tilde{\mathbf{R}}_k d(\bar{\Psi}_i)), \quad (79)$$

where $\tilde{\Psi} = \sum_{i=1}^K \bar{\Psi}_i$ and $\tilde{\mathbf{R}}_k = \bar{\mathbf{R}}_k + \frac{K\sigma^2}{\rho} \mathbf{I}_M$. Use of (68) into (79) yields

$$\begin{aligned} d(I_k) &= \text{tr}(\tilde{\Psi}d(\bar{\mathbf{R}}_k)) + \sum_{i=1}^K \text{tr}(\tilde{\mathbf{R}}_k(d(\bar{\mathbf{R}}_i)\mathbf{Q}_i\bar{\mathbf{R}}_i)) \\ &\quad - \bar{\mathbf{R}}_i\mathbf{Q}_i d(\bar{\mathbf{R}}_i)\mathbf{Q}_i\bar{\mathbf{R}}_i + \bar{\mathbf{R}}_i\mathbf{Q}_i d(\bar{\mathbf{R}}_i) \\ &\quad - 2\text{tr}(\bar{\Psi}_k(d(\bar{\mathbf{R}}_k)\mathbf{Q}_k\bar{\mathbf{R}}_k \\ &\quad - \bar{\mathbf{R}}_k\mathbf{Q}_k d(\bar{\mathbf{R}}_k)\mathbf{Q}_k\bar{\mathbf{R}}_k + \bar{\mathbf{R}}_k\mathbf{Q}_k d(\bar{\mathbf{R}}_k))) \\ &= \text{tr}(\tilde{\Psi}_k d(\bar{\mathbf{R}}_k)) + \sum_{i=1}^K \text{tr}(\tilde{\mathbf{R}}_{ki} d(\bar{\mathbf{R}}_i)) \quad (80) \\ &= \text{tr}(\tilde{\Psi}_k(d(\mathbf{R}_{0k}) + d(\mathbf{R}_{1k}))) \\ &\quad + \sum_{i=1}^K \text{tr}(\tilde{\mathbf{R}}_{ki}(d(\mathbf{R}_{0i}) + d(\mathbf{R}_{1i}))), \quad (81) \end{aligned}$$

where

$$\tilde{\Psi}_k = \bar{\Psi} - 2(\mathbf{Q}_k\bar{\mathbf{R}}_k\bar{\Psi}_k + \bar{\Psi}_k\bar{\mathbf{R}}_k\mathbf{Q}_k - \mathbf{Q}_k\bar{\mathbf{R}}_k\bar{\Psi}_k\bar{\mathbf{R}}_k\mathbf{Q}_k) \quad (82)$$

$$\tilde{\mathbf{R}}_{ki} = \mathbf{Q}_i\bar{\mathbf{R}}_i\tilde{\mathbf{R}}_k - \mathbf{Q}_i\bar{\mathbf{R}}_i\tilde{\mathbf{R}}_k\bar{\mathbf{R}}_i\mathbf{Q}_i + \tilde{\mathbf{R}}_k\bar{\mathbf{R}}_i\mathbf{Q}_i. \quad (83)$$

Equation (81) is obtained because the dependence of $\bar{\mathbf{R}}_k$ from Φ_1 is hidden only on \mathbf{R}_{0k} and \mathbf{R}_{1k} . Substitution of (70) and (72) into (95) allows to prove $\nabla_{\theta^t} I_k$ as

$$\begin{aligned} \nabla_{\bar{\theta}} I_k &= \frac{\partial}{\partial \bar{\theta}^*} I_k \\ &= \text{diag}(\bar{\nu}_{1k}\mathbf{B}_1 + \bar{\nu}_{2k}\mathbf{B}_2 + \sum_{i=1}^K (\tilde{\nu}_{ki1}\mathbf{B}_1 + \tilde{\nu}_{ki2}\mathbf{B}_2)), \quad (84) \end{aligned}$$

where $\bar{\nu}_{1k} = \bar{C}\text{tr}(\tilde{\Psi}_k\mathbf{R}_t)$, $\bar{\nu}_{2k} = \hat{\beta}_{1k}\text{tr}(\tilde{\Psi}_k\mathbf{R}_1)$, $\tilde{\nu}_{ki1} = \bar{C}\text{tr}(\tilde{\mathbf{R}}_{ki}\mathbf{R}_t)$, and $\tilde{\nu}_{ki2} = \hat{\beta}_{1k}\text{tr}(\tilde{\mathbf{R}}_{ki}\mathbf{R}_1)$.

APPENDIX D PROOF OF PROPOSITION 3

In the case of the STAR-RIS, we have to derive $\nabla_{\theta^t} \text{SE}(\theta, \beta)$ in terms of θ^{t*} , which is written as

$$\nabla_{\theta^t} \text{SE}(\theta, \beta) = c \sum_{k=1}^K \frac{I_k \nabla_{\theta^t} S_k - S_k \nabla_{\theta^t} I_k}{(1 + \gamma_k) I_k^2}, \quad (85)$$

where $c = \frac{\tau_c - \tau}{\tau_c \log_2(e)}$.

Regarding the computation of $\nabla_{\theta^t} S_k$, we observe that $\nabla_{\theta^t} S_k = 0$ if $w_k = r$, i.e., when UE k is in the reflection region. Hence, we focus on the derivation of $\nabla_{\theta^t} S_k$ when $w_k = t$, which requires the derivation of $d(S_k)$. Similar to (62), we have

$$d(S_k) = 2\text{tr}(\bar{\Psi}_k)\text{tr}(d(\bar{\Psi}_k)) \quad (86)$$

with $\bar{\Psi}_k$ written as in (64). Note that, in $\bar{\Psi}_k$, only \mathbf{R}_{0k} and \mathbf{R}_{2k} depend on Φ_{2,w_k} . Thus, its differential is obtained as

$$\begin{aligned} d(\bar{\Psi}_k) &= d(\mathbf{R}_{0k})\mathbf{Q}_{0k}\mathbf{R}_{0k} - \mathbf{R}_{0k}\mathbf{Q}_{1k}d(\mathbf{R}_{1k})\mathbf{Q}_{1k}\mathbf{R}_{0k} \\ &\quad + \mathbf{R}_{0k}\mathbf{Q}_{0k}d(\mathbf{R}_{0k}) + d(\mathbf{R}_{2k})\mathbf{Q}_{2k}\mathbf{R}_{2k} \\ &\quad - \mathbf{R}_{2k}\mathbf{Q}_{2k}d(\mathbf{R}_{2k})\mathbf{Q}_{2k}\mathbf{R}_{2k} + \mathbf{R}_{2k}\mathbf{Q}_{2k}d(\mathbf{R}_{2k}), \quad (87) \end{aligned}$$

where $\mathbf{R}_{0k} = \bar{\mathbf{D}}\text{tr}(\mathbf{B}_{3t}\Phi_{2,t}^H)$ and $\mathbf{R}_{2k} = \text{tr}(\mathbf{B}_{4t}\Phi_{2,t}^H)\mathbf{R}_2$ with $\mathbf{B}_{3t} = \mathbf{R}_1\Phi_{2,t}\mathbf{R}_2$, $\bar{\mathbf{D}} = \text{tr}(\mathbf{B}_1\Phi_1^H)\mathbf{R}_t$, and $\mathbf{B}_{4t} = \hat{\beta}_{2k}\text{tr}(\mathbf{R}_t\Phi_{2,t}\mathbf{R}_2)$.

The differentials of \mathbf{R}_{0k} and \mathbf{R}_{2k} are derived as

$$\begin{aligned} d(\mathbf{R}_{0k}) &= \bar{\mathbf{D}}((\text{diag}(\mathbf{B}_{3t}^H \text{diag}(\beta^t)))^\top d(\theta^t) \\ &\quad + (\text{diag}(\mathbf{B}_{3t} \text{diag}(\beta^t)))^\top d(\theta^{t*})), \quad (88) \end{aligned}$$

$$\begin{aligned} d(\mathbf{R}_{2k}) &= \mathbf{R}_2((\text{diag}(\mathbf{B}_{4t}^H \text{diag}(\beta^t)))^\top d(\theta^t) \\ &\quad + (\text{diag}(\mathbf{B}_{4t} \text{diag}(\beta^t)))^\top d(\theta^{t*})). \quad (89) \end{aligned}$$

Based on (88) and (89), (86) becomes

$$\begin{aligned} d(S_k) - 2\text{tr}(\bar{\Psi}_k)\text{tr}(\mathbf{Q}_{0k}\mathbf{R}_{0k}d(\mathbf{R}_{0k}) - \mathbf{Q}_{1k}\mathbf{R}_{0k}^2\mathbf{Q}_{1k}d(\mathbf{R}_{1k}) \\ + \mathbf{R}_{0k}\mathbf{Q}_{0k}d(\mathbf{R}_{0k}) + \mathbf{Q}_{2k}\mathbf{R}_{2k}d(\mathbf{R}_{2k}) \\ - \mathbf{Q}_{2k}\mathbf{R}_{2k}^2\mathbf{Q}_{2k}d(\mathbf{R}_{2k}) + \mathbf{R}_{2k}\mathbf{Q}_{2k}d(\mathbf{R}_{2k})) \\ = \nu_{2k}(\text{diag}((\mathbf{B}_{3t}^H \text{diag}(\beta^t)))^\top d\theta^t \\ + (\text{diag}(\mathbf{B}_{3t} \text{diag}(\beta^t)))^\top d\theta^{t*}) \\ + \nu_{3k}(\text{diag}((\mathbf{B}_{4t}^H \text{diag}(\beta^t)))^\top d\theta^t \\ + (\text{diag}(\mathbf{B}_{4t} \text{diag}(\beta^t)))^\top d\theta^{t*}), \quad (90) \end{aligned}$$

where

$$\nu_{2k} = 2\text{tr}(\bar{\Psi}_k)\text{tr}(\mathbf{Q}_{0k}\mathbf{R}_{0k}\bar{\mathbf{D}} - \mathbf{Q}_{1k}\mathbf{R}_{0k}^2\mathbf{Q}_{1k}\bar{\mathbf{D}} + \mathbf{R}_{0k}\mathbf{Q}_{0k}\bar{\mathbf{D}}), \quad (92)$$

$$\begin{aligned} \nu_{3k} &= 2\text{tr}(\bar{\Psi}_k)\text{tr}(\mathbf{Q}_{2k}\mathbf{R}_{2k}\mathbf{R}_2 - \mathbf{Q}_{2k}\mathbf{R}_{2k}^2\mathbf{Q}_{2k}\mathbf{R}_2 \\ &\quad + \mathbf{R}_{2k}\mathbf{Q}_{2k}\mathbf{R}_2). \quad (93) \end{aligned}$$

Thus, in the case of $w_k = t$, we obtain

$$\nabla_{\theta^t} S_k = \nu_{2k}\text{diag}(\mathbf{B}_{3t}\text{diag}(\beta^t)) + \nu_{3k}\text{diag}(\mathbf{B}_{4t}\text{diag}(\beta^t)), \quad (94)$$

which equals to (44a). The proof of (44b) follows similar lines.

To derive $\nabla_{\theta} I_k$, we aim at finding the differential of I_k . In a similar way to (79), we obtain

$$\begin{aligned} d(I_k) &= \text{tr}(\tilde{\Psi}_k(d(\mathbf{R}_{0k}) + d(\mathbf{R}_{2k}))) \\ &\quad + \sum_{i \in \mathcal{K}_t} \text{tr}(\tilde{\mathbf{R}}_{ki}(d(\mathbf{R}_{0i}) + d(\mathbf{R}_{2i}))), \quad (95) \end{aligned}$$

Note that $d(\mathbf{R}_{0i}) = d(\mathbf{R}_{2i}) = 0$ if $w_i \neq t$ because $d(\mathbf{R}_{0i})$ and $d(\mathbf{R}_{2i})$ do not depend on θ^t in this case. Hence, we have

$$\nabla_{\theta^t} I_k = \frac{\partial}{\partial \theta^{t*}} I_k$$

$$= \text{diag}(\tilde{\mathbf{A}}_{kt} \text{diag}(\boldsymbol{\beta}^t)), \quad (96)$$

where

$$\tilde{\mathbf{A}}_{kt} = \begin{cases} \bar{v}_{2k} \mathbf{B}_3 + \bar{v}_{2k} \mathbf{B}_4 + \sum_{i \in \mathcal{K}_t} (\tilde{v}_{ki2} \mathbf{B}_3 + \tilde{v}_{ki2} \mathbf{B}_4) & w_k = t \\ \sum_{i \in \mathcal{K}_t} (\tilde{v}_{ki2} \mathbf{B}_3 + \tilde{v}_{ki2} \mathbf{B}_4) & w_k \neq t \end{cases} \quad (97)$$

with $\bar{v}_{1k} = \text{tr}(\tilde{\Psi}_k \bar{\mathbf{D}})$, $\bar{v}_{2k} = \hat{\beta}_{1k} \text{tr}(\tilde{\Psi}_k \mathbf{R}_2)$, $\tilde{v}_{ki1} = \text{tr}(\tilde{\mathbf{R}}_{ki} \bar{\mathbf{D}})$, and $\tilde{v}_{ki2} = \hat{\beta}_{1k} \text{tr}(\tilde{\mathbf{R}}_{ki} \mathbf{R}_2)$. Thus, (44c) is proved, while (44d) is obtained by following the same steps.

In the case of $\nabla_{\boldsymbol{\beta}^t} S_k$, we consider first the scenario $w_k = t$, and we have

$$d(\mathbf{R}_{0k}) = 2\text{Re}\{\bar{\mathbf{D}}(\text{diag}(\mathbf{B}_{3t}^H \text{diag}(\boldsymbol{\beta}^t)))\}^T d(\boldsymbol{\theta}^t), \quad (98)$$

$$d(\mathbf{R}_{2k}) = 2\text{Re}\{\mathbf{R}_2(\text{diag}(\mathbf{B}_{4t}^H \text{diag}(\boldsymbol{\beta}^t)))\}^T d(\boldsymbol{\theta}^t). \quad (99)$$

By substituting (98) and (99) into (86), we obtain

$$\begin{aligned} \nabla_{\boldsymbol{\theta}^t} S_k &= 2\text{Re}\{\bar{\mathbf{D}}(\text{diag}(\mathbf{B}_{3t}^H \text{diag}(\boldsymbol{\beta}^t)))\} \\ &\quad + 2\text{Re}\{\mathbf{R}_2(\text{diag}(\mathbf{B}_{4t}^H \text{diag}(\boldsymbol{\beta}^t)))\}. \end{aligned} \quad (100)$$

Following the same lines as above, we result in

$$\begin{aligned} \nabla_{\boldsymbol{\theta}^r} S_k &= 2\text{Re}\{\bar{\mathbf{D}}(\text{diag}(\mathbf{B}_{3r}^H \text{diag}(\boldsymbol{\beta}^r)))\} \\ &\quad + 2\text{Re}\{\mathbf{R}_2(\text{diag}(\mathbf{B}_{4r}^H \text{diag}(\boldsymbol{\beta}^r)))\}, \end{aligned} \quad (101)$$

$$\nabla_{\boldsymbol{\theta}^t} I_k = 2\text{Re}\{\text{diag}(\tilde{\mathbf{A}}_{kt} \text{diag}(\boldsymbol{\beta}^t))\}, \quad (102)$$

$$\nabla_{\boldsymbol{\theta}^r} I_k = 2\text{Re}\{\text{diag}(\tilde{\mathbf{A}}_{kr} \text{diag}(\boldsymbol{\beta}^r))\}, \quad (103)$$

which concludes the proof.

REFERENCES

- [1] Q. Wu and R. Zhang, "Towards smart and reconfigurable environment: Intelligent reflecting surface aided wireless network," *IEEE Commun. Mag.*, vol. 58, no. 1, pp. 106–112, Jan. 2020.
- [2] M. Di Renzo et al., "Smart radio environments empowered by reconfigurable intelligent surfaces: How it works, state of research, and the road ahead," *IEEE J. Sel. Areas Commun.*, vol. 38, no. 11, pp. 2450–2525, Nov. 2020.
- [3] Q. Wu and R. Zhang, "Intelligent reflecting surface enhanced wireless network via joint active and passive beamforming," *IEEE Trans. Wireless Commun.*, vol. 18, no. 11, pp. 5394–5409, Nov. 2019.
- [4] A. Papazafeiropoulos, P. Kourtessis, K. Ntontin, and S. Chatzinotas, "Joint spatial division and multiplexing for FDD in intelligent reflecting surface-assisted massive MIMO systems," *IEEE Trans. Veh. Technol.*, vol. 71, no. 10, pp. 10754–10769, Oct. 2022.
- [5] A. Papazafeiropoulos, I. Krikidis, and P. Kourtessis, "Impact of channel aging on reconfigurable intelligent surface aided massive MIMO systems with statistical CSI," *IEEE Trans. Veh. Technol.*, vol. 72, no. 1, pp. 689–703, Jan. 2023.
- [6] B. Zheng and R. Zhang, "Intelligent reflecting surface-enhanced OFDM: Channel estimation and reflection optimization," *IEEE Wireless Commun. Lett.*, vol. 9, no. 4, pp. 518–522, Apr. 2020.
- [7] Y. Yang, B. Zheng, S. Zhang, and R. Zhang, "Intelligent reflecting surface meets OFDM: Protocol design and rate maximization," *IEEE Trans. Commun.*, vol. 68, no. 7, pp. 4522–4535, Jul. 2020.
- [8] B. Zheng and R. Zhang, "IRS meets relaying: Joint resource allocation and passive beamforming optimization," *IEEE Wireless Commun. Lett.*, vol. 10, no. 9, pp. 2080–2084, Sep. 2021.
- [9] I. Yildirim, F. Kilinc, E. Basar, and G. C. Alexandropoulos, "Hybrid RIS-empowered reflection and decode-and-forward relaying for coverage extension," *IEEE Commun. Lett.*, vol. 25, no. 5, pp. 1692–1696, May 2021.
- [10] T. Hou, Y. Liu, Z. Song, X. Sun, and Y. Chen, "MIMO-NOMA networks relying on reconfigurable intelligent surface: A signal cancellation-based design," *IEEE Trans. Commun.*, vol. 68, no. 11, pp. 6932–6944, Nov. 2020.
- [11] B. Zheng, C. You, and R. Zhang, "Double-IRS assisted multi-user MIMO: Cooperative passive beamforming design," *IEEE Trans. Wireless Commun.*, vol. 20, no. 7, pp. 4513–4526, Jul. 2021.
- [12] B. Zheng, C. You, and R. Zhang, "Efficient channel estimation for double-IRS aided multi-user MIMO system," *IEEE Trans. Commun.*, vol. 69, no. 6, pp. 3818–3832, Jun. 2021.
- [13] W. Mei, B. Zheng, C. You, and R. Zhang, "Intelligent reflecting surface-aided wireless networks: From single-reflection to multireflection design and optimization," *Proc. IEEE*, vol. 110, no. 9, pp. 1380–1400, Sep. 2022.
- [14] L. Dong, H.-M. Wang, J. Bai, and H. Xiao, "Double intelligent reflecting surface for secure transmission with inter-surface signal reflection," *IEEE Trans. Veh. Technol.*, vol. 70, no. 3, pp. 2912–2916, Mar. 2021.
- [15] Z. Abdullah, A. Papazafeiropoulos, S. Kisseleff, S. Chatzinotas, and B. Ottersten, "Impact of phase-noise and spatial correlation on double-RIS-assisted multiuser MISO networks," *IEEE Wireless Commun. Lett.*, vol. 11, no. 7, pp. 1473–1477, Jul. 2022.
- [16] A. Papazafeiropoulos, P. Kourtessis, S. Chatzinotas, and J. M. Senior, "Coverage probability of double-IRS assisted communication systems," *IEEE Wireless Commun. Lett.*, vol. 11, no. 1, pp. 96–100, Jan. 2022.
- [17] G. Ding, F. Yang, L. Ding, and Y. Cui, "Analysis and optimization of a double-IRS cooperatively assisted system with a quasi-static phase shift design," *IEEE Trans. Wireless Commun.*, vol. 22, no. 7, pp. 4416–4433, Jul. 2023.
- [18] Y. Han, S. Zhang, L. Duan, and R. Zhang, "Double-IRS aided MIMO communication under LoS channels: Capacity maximization and scaling," *IEEE Trans. Commun.*, vol. 70, no. 4, pp. 2820–2837, Apr. 2022.
- [19] Y. Han, S. Zhang, L. Duan, and R. Zhang, "Cooperative double-IRS aided communication: Beamforming design and power scaling," *IEEE Wireless Commun. Lett.*, vol. 9, no. 8, pp. 1206–1210, Aug. 2020.
- [20] J. Xu, Y. Liu, X. Mu, and O. A. Dobre, "STAR-RISs: Simultaneous transmitting and reflecting reconfigurable intelligent surfaces," *IEEE Commun. Lett.*, vol. 25, no. 9, pp. 3134–3138, Sep. 2021.
- [21] X. Mu, Y. Liu, L. Guo, J. Lin, and R. Schober, "Simultaneously transmitting and reflecting (STAR) RIS aided wireless communications," *IEEE Trans. Wireless Commun.*, vol. 21, no. 5, pp. 3083–3098, May 2022.
- [22] A. Papazafeiropoulos, P. Kourtessis, and I. Krikidis, "STAR-RIS assisted full-duplex systems: Impact of correlation and maximization," *IEEE Commun. Lett.*, vol. 26, no. 12, pp. 3004–3008, Dec. 2022.
- [23] A. Papazafeiropoulos, Z. Abdullah, P. Kourtessis, S. Kisseleff, and I. Krikidis, "Coverage probability of STAR-RIS-Assisted massive MIMO systems with correlation and phase errors," *IEEE Wireless Commun. Lett.*, vol. 11, no. 8, pp. 1738–1742, Aug. 2022.
- [24] H. Niu, Z. Chu, F. Zhou, P. Xiao, and N. Al-Dhahir, "Weighted sum rate optimization for STAR-RIS-assisted MIMO system," *IEEE Trans. Veh. Technol.*, vol. 71, no. 2, pp. 2122–2127, Feb. 2022.
- [25] J. Xu, Y. Liu, X. Mu, R. Schober, and H. V. Poor, "STAR-RISs: A correlated T&R phase-shift model and practical phase-shift configuration strategies," *IEEE J. Sel. Topics Signal Process.*, vol. 16, no. 5, pp. 1097–1111, Aug. 2022.
- [26] H. Zhang et al., "Intelligent omni-surfaces for full-dimensional wireless communications: Principles, technology, and implementation," *IEEE Commun. Mag.*, vol. 60, no. 2, pp. 39–45, Feb. 2022.
- [27] S. Zeng et al., "Intelligent omni-surfaces: Reflection-refraction circuit model, full-dimensional beamforming, and system implementation," *IEEE Trans. Commun.*, vol. 70, no. 11, pp. 7711–7727, Nov. 2022.
- [28] S. Zhang, H. Zhang, B. Di, Y. Tan, Z. Han, and L. Song, "Beyond intelligent reflecting surfaces: Reflective-transmissive metasurface aided communications for full-dimensional coverage extension," *IEEE Trans. Veh. Technol.*, vol. 69, no. 11, pp. 13905–13909, Nov. 2020.
- [29] C. Pan et al., "Multicell MIMO communications relying on intelligent reflecting surfaces," *IEEE Trans. Wireless Commun.*, vol. 19, no. 8, pp. 5218–5233, Aug. 2020.
- [30] E. Björnson and L. Sanguinetti, "Rayleigh fading modeling and channel hardening for reconfigurable intelligent surfaces," *IEEE Wireless Commun. Lett.*, vol. 10, no. 4, pp. 830–834, Apr. 2021.
- [31] T. Badloe, J. Mun, and J. Rho, "Metasurfaces-based absorption and reflection control: Perfect absorbers and reflectors," *J. Nanomater.*, vol. 2017, 2017.
- [32] J. Hoydis, S. ten Brink, and M. Debbah, "Massive MIMO in the UL/DL of cellular networks: How many antennas do we need?," *IEEE J. Select. Areas Commun.*, vol. 31, no. 2, pp. 160–171, Feb. 2013.
- [33] D. Neumann, M. Joham, and W. Utschick, "Covariance matrix estimation in massive MIMO," *IEEE Signal Process. Lett.*, vol. 25, no. 6, pp. 863–867, Jun. 2018.

- [34] A. Papazafeiropoulos, "Ergodic capacity of IRS-assisted MIMO systems with correlation and practical phase-shift modeling," *IEEE Wireless Commun. Lett.*, vol. 11, no. 2, pp. 421–425, Feb. 2022.
- [35] E. Björnson et al., "Massive MIMO networks: Spectral, energy, and hardware efficiency," *Found. Trends Signal Process.*, vol. 11, no. 3/4, pp. 154–655, 2017.
- [36] F. Jiang et al., "Optimization of RIS-aided integrated localization and communication," 2022, *arXiv:2209.02828*.
- [37] Z.-Q. He and X. Yuan, "Cascaded channel estimation for large intelligent metasurface assisted massive MIMO," *IEEE Wireless Commun. Lett.*, vol. 9, no. 2, pp. 210–214, Feb. 2019.
- [38] Q. U. A. Nadeem et al., "Intelligent reflecting surface-assisted multi-user MISO communication: Channel estimation and beamforming design," *IEEE Open J. Commun. Soc.*, vol. 1, pp. 661–680, 2020.
- [39] M. Medard, "The effect upon channel capacity in the wireless communications of perfect and imperfect knowledge of the channel," *IEEE Trans. Inf. Theory*, vol. 46, no. 3, pp. 933–946, May 2000.
- [40] R. Couillet and M. Debbah, *Random Matrix Methods for Wireless Communications*. Cambridge, U.K.: Cambridge Univ. Press, 2011.
- [41] D. P. Bertsekas, *Nonlinear Programming*, Cambridge, MA, USA: MIT Press, 1999.
- [42] A. K. Papazafeiropoulos and T. Ratnarajah, "Deterministic equivalent performance analysis of time-varying massive MIMO systems," *IEEE Trans. Wireless Commun.*, vol. 14, no. 10, pp. 5795–5809, Oct. 2015.
- [43] A. Hjørungnes, *Complex-Valued Matrix Derivatives: With Applications in Signal Processing and Communications*. Cambridge, U.K.: Cambridge Univ. Press, 2011.



Anastasios Papazafeiropoulos (Senior Member, IEEE) received the B.Sc. degree (Hons.) in physics, the M.Sc. degree (Hons.) in electronics and computers science, and the Ph.D. degree from the University of Patras, Greece, in 2003, 2005, and 2010, respectively. From 2011 to 2012 and from 2016 to 2017, he was with the Institute for Digital Communications with The University of Edinburgh, Edinburgh, U.K., as a Post-Doctoral Research Fellow. From 2012 to 2014, he was a Research Fellow with Imperial College London, London, U.K., awarded with a Marie Curie

Fellowship (IEF-IAWICOM). He is currently a Vice-Chancellor Fellow with the University of Hertfordshire, Hatfield, U.K. He is also a Visiting Research Fellow with the SnT, University of Luxembourg, Esch-sur-Alzette, Luxembourg. He has been involved in several EPSRC and EU FP7 projects such as HIATUS and HARP. His research interests span machine learning for wireless communications, intelligent reflecting surfaces, massive MIMO, heterogeneous networks, 5G and beyond wireless networks, full-duplex radio, mm-wave communications, random matrix theory, hardware-constrained communications, and performance analysis of fading channels.



Ahmet M. Elbir (Senior Member, IEEE) received the B.S. degree (with Hons.) in electrical engineering from Firat University, Elazığ, Turkey, in 2009 and the Ph.D. degree in electrical engineering from Middle East Technical University (METU), Ankara, Turkey, in 2016. He has held Visiting Postdoctoral Researcher positions at Koc University, Istanbul, Turkey, during 2020–2021, and Carleton University, Ottawa, ON, Canada during 2022–2023. He was a Senior Researcher with Duzce University, Duzce, Turkey, during 2016–2022. He is currently a Research Fel-

low with the University of Luxembourg, Esch-sur-Alzette, Luxembourg, and University of Hertfordshire, Hertfordshire, U. K. He was the recipient of 2016 METU best Ph.D. thesis award for his doctoral studies, and the IET Radar, Sonar and Navigation Best Paper Award in 2022. He has been a Member of IEEE Signal Processing Society Technical Working Group on synthetic apertures since 2022, and Associate Editor for IEEE ACCESS since 2018, and the Lead Guest Editor of IEEE JOURNAL OF SELECTED TOPICS ON SIGNAL PROCESSING and IEEE WIRELESS COMMUNICATIONS. His research interests include array signal processing, sparsity-driven convex optimization, signal processing for communications and deep learning for array signal processing.



Pandelis Kourtessis is currently a Director of the Centre for Engineering Research and Reader in Communication Networks with the University of Hertfordshire, Hertfordshire, U.K., leading the activities of the Networks Engineering Research Group into Communications and Information engineering, including Next Generation Passive Optical Networks, Optical and Wireless MAC Protocols, 5G RANs, Software Defined Network and Network Virtualization 5G and Satellite Networks and more recently Machine Learning for Next Generation Networks.

His funding ID includes EU COST, FP7, H2020, European Space Agency (ESA), UKRI and industrially funded projects. He was a General Chair, CoChair, technical programme committee Member and at the scientific committees and expert Groups of IEEE workshops and conferences, European Technology Platforms and European Networks of Excellence. He has authored or coauthored more than 80 papers at peer-reviewed journals, peer-reviewed conference proceedings and international conferences. His research has received coverage at scientific journals, magazines, white papers and international workshops. He co-editor of a Springer book and Chapter Editor of an IET book on softwarization for 5G.



Ioannis Krikidis (Fellow, IEEE) received the Diploma degree in computer engineering from the Computer Engineering and Informatics Department, University of Patras, Patras, Greece, in 2000, and the M.Sc. and Ph.D. degrees in electrical engineering from École Nationale Supérieure des Télécommunications (ENST), Paris, France, in 2001 and 2005, respectively. From 2006 to 2007, he was a Postdoctoral Researcher with ENST, Paris. From 2007 to 2010, he was a Research Fellow with the School of Engineering and Electronics, The University of Edinburgh,

Edinburgh, U.K. He also has held research positions at the Department of Electrical Engineering, University of Notre Dame, Notre Dame, IN, USA, the Department of Electrical and Computer Engineering, University of Maryland, College Park, MD, USA, the Interdisciplinary Centre for Security, Reliability and Trust, University of Luxembourg, and the Department of Electrical and Electronic Engineering, Niigata University, Niigata, Japan. He is currently an Associate Professor with the Department of Electrical and Computer Engineering, University of Cyprus, Nicosia, Cyprus. His research interests include wireless communications, cooperative networks, 6G communication systems, wireless powered communications, and intelligent reflecting surfaces. He is an Associate Editor for IEEE TRANSACTIONS ON WIRELESS COMMUNICATIONS, and the Senior Editor of IEEE WIRELESS COMMUNICATIONS LETTERS. He was the recipient of the Young Researcher Award from the Research Promotion Foundation, Cyprus, in 2013, and IEEE ComSoc Best Young Professional Award in Academia, 2016. He has been recognized by the Web of Science as a Highly Cited Researcher for 2017 to 2021, and the prestigious ERC Consolidator Grant.



Symeon Chatzinotas (Fellow, IEEE) is currently a Full Professor / Chief Scientist I and Head of the SIGCOM Research Group at SnT, University of Luxembourg. He is coordinating the research activities on communications and networking, acting as a PI for more than 20 projects and main representative for 3GPP, ETSI, DVB. In the past, he has been a Visiting Professor with the University of Parma, Parma, Italy, lecturing on 5G Wireless Networks. He was involved in numerous R&D projects for NCSR Demokritos, CERTH Hellas and CCSR, University of Surrey. He

was the co-recipient of the 2014 IEEE Distinguished Contributions to Satellite Communications Award and Best Paper Awards at EURASIP JWCN, CROWN-COM, ICSSC. He has (co-)authored more than 450 technical papers in refereed international journals, conferences and scientific books. He is currently with the Editorial board of the IEEE TRANSACTIONS ON COMMUNICATIONS, IEEE OPEN JOURNAL OF VEHICULAR TECHNOLOGY and the *International Journal of Satellite Communications and Networking*.